Mapping the immunogenic landscape of near-native HIV-1 envelope trimers in non-human primates

Christopher A. Cottrell[1,2,3], Jelle van Schooten[4], Charles A. Bowman[1], Meng Yuan[1], David Oyen[1], Mia Shin[1], Robert Morpurgo[4], Patricia van der Woude[4], Marielle van Breemen[4], Jonathan L. Torres[1], Raj Patel[1], Justin Gross[1], Leigh M. Sewall[1], Jeffrey Copps[1], Gabriel Ozorowski[1,2,3], Bartek Nogal[1,2,3], Devin Sok[2,3,5], Eva G. Rakasz[6], Celia Labranche[7], Vladimir Vigdorovich[12], Scott Christley[13], Diane G. Carnathan[3,14], D. Noah Sather[12], David Montefiori[7,8], Guido Silvestri[3,14], Dennis R. Burton[2,3,5,9], John P. Moore[10], Ian A. Wilson[1,2,3,11], Rogier W. Sanders[1,10#], Andrew B. Ward[1,2,3#], Marit J. van Gils[4#]

[1] Department of Integrative Structural and Computational Biology, The Scripps Research Institute, La Jolla, CA 92037, USA.

[2] IAVI Neutralizing Antibody Center, The Scripps Research Institute, La Jolla, CA 92037, USA.

[3] Consortium for HIV/AIDS Vaccine Development, The Scripps Research Institute, La Jolla, CA 92037, USA.

[4] Department of Medical Microbiology, Amsterdam UMC, University of Amsterdam, 1105 AZ Amsterdam, The Netherlands.

[5] Department of Immunology and Microbiology, The Scripps Research Institute, La Jolla, CA 92037, USA.

[6] Wisconsin National Primate Research Center, University of Wisconsin, Madison, WI 53715, USA.

[7] Department of Surgery, Duke University Medical Center, Durham, NC 27710, USA.

[8] Duke Human Vaccine Institute, Duke University Medical Center, Durham, NC 27710, USA.

23 [9] The Ragon Institute of Massachusetts General Hospital, Massachusetts Institute of Technology
24 and Harvard University, Cambridge, MA 02139, USA.
25 [10] Department of Microbiology and Immunology, Weill Medical College of Cornell University, New
26 York, NY 10021,USA
27 [11] The Skaggs Institute for Chemical Biology, The Scripps Institute, La Jolla, CA 92037, USA
28 [12] Center for Global Infectious Disease Research, Seattle Children's Research Institute, Seattle,
29 WA 98109, USA.
30 [13] Department of Population and Data Sciences, UT Southwestern Medical Center, Dallas, TX
31 75390, USA
32 [14] Yerkes National Primate Research Center, Emory University, Atlanta, GA 30322, USA;
33
34 [#] corresponding author; m.j.vangils@amc.uva.nl; andrew@scripps.edu; r.w.sanders@amc.uva.nl

Summary

The induction of broad and potent immunity by vaccines is the key focus of research efforts aimed at protecting against HIV-1 infection. Soluble native-like HIV-1 envelope glycoproteins have shown promise as vaccine candidates as they can induce potent autologous neutralizing responses in rabbits and non-human primates. In this study, monoclonal antibodies were isolated and characterized from rhesus macaques immunized with the BG505 SOSIP.664 trimer to better understand vaccine-induced antibody responses. Our studies reveal a diverse landscape of antibodies recognizing immunodominant strain-specific epitopes and non-neutralizing neo-epitopes. Additionally, we isolated a subset of mAbs against an epitope cluster at the gp120-gp41 interface that recognize the highly conserved fusion peptide and the glycan at position 88 and have characteristics akin to several human-derived broadly neutralizing antibodies.

47 **Introduction**

48 HIV-1 continues to cause significant morbidity and mortality around the world with an estimated
49 1.7 million new infections in 2018 (UNAIDS, 2019), which emphasizes the need for an effective
50 prophylactic vaccine. The HIV-1 envelope glycoprotein (Env) is the sole target for neutralizing
51 antibody (NAb) responses. Studies of infected patients have led to the isolation of NAbs against
52 multiple different epitopes on the Env surface that are capable of both neutralizing most
53 circulating strains and providing passive protection against repeated viral challenges in non-
54 human primates (NHPs) (Burton and Hangartner, 2016; Moldt et al., 2016; Pegu et al., 2019; Wu,
55 2018). Extensive research efforts, including structure-based engineering of Env immunogens, are
56 currently directed towards developing vaccine strategies to successfully elicit broadly
57 neutralizing antibodies (bNAbs) against specific Env epitopes (de Taeye et al., 2015; Escolano et
58 al., 2019; Escolano et al., 2016; Jardine et al., 2016; Kong et al., 2019; Steichen et al., 2016;
59 Torrents de la Pena et al., 2017). The development and structural determination of soluble
60 native-like Env trimer mimics, particularly ones based on the SOSIP technology, has provided a
61 platform for structure-based immunogen design (Julien et al., 2013a; Lyumkis et al., 2013;
62 Pancera et al., 2014; Sanders et al., 2013). NAbs induced by SOSIP trimers in NHPs can protect
63 against challenge with an autologous Simian-Human Immunodeficiency virus (SHIV) (Pauthner et
64 al., 2017; Pauthner et al., 2019). However, as NAbs with the required breadth of activity have not
65 yet been induced in trimer-immunized animals, improvements to current vaccine design and
66 delivery strategies are clearly needed.

67 Characterizing the antibody response to SOSIP trimers may provide useful information for
68 guiding immunogen design. Initial analyses of rabbits immunized with BG505 SOSIP.664 trimers,

69 including studies of isolated monoclonal antibodies (mAbs), showed that autologous NAbs
70 targeted a large hole in the glycan shield of the BG505 virus caused by the absence of
71 glycosylation sites at positions 241 and 289 (Klasse et al., 2018; McCoy et al., 2016). The 241
72 glycan is highly conserved (97%) among HIV-1 strains and while the 289 glycan is less conserved,
73 it is still present in 79% of viruses. The required absence of typically conserved glycans explains
74 why the NAbs isolated from the trimer-immunized rabbits lack breadth (McCoy et al., 2016). Later
75 studies involving BG505 trimer-immunized rabbits, guinea pigs, and NHPs have identified
76 additional narrow-specificity neutralizing serum responses that recognize epitopes in the C3/V4,
77 C3/V5, and V1 regions, with mAbs isolated from guinea pigs targeting the C3/V4 epitope (Cirelli
78 et al., 2019; Klasse et al., 2018; Lei et al., 2019; Nogal et al., 2019; Pauthner et al., 2017).
79 Here, we describe a detailed characterization of neutralizing and non-neutralizing mAbs
80 isolated from two rhesus macaques (RMs) previously immunized with the BG505 SOSIP.664
81 trimer (Sanders et al., 2015). We identified multiple mAbs targeting the 289-glycan hole on the
82 BG505 SOSIP.664 trimer or a neo-epitope cluster at the base of the trimer. The most potent NAb
83 isolated targeted the gp120/gp41 interface at an epitope that significantly overlaps with the
84 epitope of human bNAb VRC34 (Kong et al., 2016). Insights from the induction of these NAbs
85 through vaccination can be further used to develop immunogens and immunization strategies to
86 induce cross-reactive antibody responses.
87

88 **Results**

89 **Indian origin rhesus macaque BCR germline database**

90 The majority of bNAbs isolated from HIV-infected patients have exceedingly high levels of
91 somatic hypermutation (SHM) (Landais and Moore, 2018; Wu, 2018). Accurately measuring levels
92 of SHM elicited during immunization experiments is a critical component to ensuring the elicited
93 antibodies are acquiring the level of mutations associated with neutralization breadth. To
94 accurately measure the extent of SHM, the mAb sequences that we obtained from BG505
95 SOSIP.664 trimer-immunized RMs required comparison to a germline B-cell receptor (BCR)
96 reference database. The IMGT reference database for RMs is incomplete and contains a mixture
97 of genes/alleles from both Chinese and Indian origin animals. Given the high levels of genetic
98 diversity in the Immunoglobulin (Ig) loci among RMs from different origins (Corcoran et al., 2016)
99 and the general use of Indian origin RMs in most HIV-1 immunization experiments conducted in
100 the United States, we constructed a germline database containing gene/alleles from only Indian
101 origin RMs. The gene/alleles from the published database (Vigdorovich et al., 2016) were aligned
102 to the Mmul_8.0.1 Indian origin RM genome assembly using BLAST (Johnson et al., 2008; Zimin
103 et al., 2014). Sequences that were not identical to the reference genome were eliminated.
104 Additional genes/alleles from publicly available Indian origin RM genomic DNA sequencing
105 datasets (Cirelli et al., 2019; Ramesh et al., 2017) were added to the database. After duplicates
106 were removed, the resulting new database contained 189 IGHV, 70 IGHD, 9 IGHJ, 188 IGKV, 5
107 IGKJ, 147 IGLV, and 13 IGLJ genes/alleles (Table S1).

108 Recent advances in BCR repertoire sequencing and analysis have enabled the use of next-
109 generation sequencing (NGS) datasets for inferring novel genes/alleles (Corcoran et al., 2016;

110 Gadala-Maria et al., 2015; Ralph and Matsen, 2018). Using the database described above as an
111 initial database, we performed IgDiscover analysis (Corcoran et al., 2016) on IgM BCR sequences
112 derived from five Indian origin RMs. Additionally, we performed IgDiscover analysis on previously
113 obtained Indian origin RM BCR NGS datasets that were downloaded from the NCBI sequence read
114 archive (Corcoran et al., 2016; Guo et al., 2015) or obtained directly from the study authors
115 (Vigdorovich et al., 2016). Inferred genes/alleles were kept if they were detected in more than
116 one animal or if they were identical to RM genes/alleles that were previously deposited in the
117 NCBI database. We added 113 IGHV, 18 IGKV, and 18 IGLV genes/alleles to our germline database
118 (http://ward.scripps.edu/gld/) resulting in a total of 302 IGHV, 206 IGKV, and 165 IGLV
119 genes/alleles. This updated database was then converted into a custom IgBLAST database and
120 subsequently used to analyze our BG505-specific mAbs sequences with IgBLAST (Ye et al., 2013).
121

122 **Antigen-specific mAbs isolated from BG505 SOSIP.664 trimer-immunized RMs**

123 To better understand the immunogenicity of the BG505 SOSIP.664 trimers in previously
124 immunized Indian origin RMs (Sanders et al., 2015) we selected the two animals (rh1987 and
125 rh2011) with the highest serum neutralization activity against the autologous BG505.T332N
126 pseudovirus for in-depth mAb analysis. Peripheral blood mononuclear cells (PBMCs) from the
127 following time points were selected for BG505 SOSIP.664 trimer-specific IgG-positive single
128 memory B-cell sorting: (i) two weeks prior to the fourth immunization (week 22), (ii) 1 week after
129 the fourth immunization (week 25) and (iii) 1 week after the sixth immunization (week 53) (Fig
130 1A). In total, 25 and 17 mAbs were cloned from RMs rh1987 and rh2011, respectively (Fig 1B).

131 The BG505-specific mAb sequences were analysed using our germline database and
132 shown to be evenly distributed between kappa and lambda light chains (KC and LC) usage (Fig
133 1B). For animal rh1987, 11 KC and 14 LC mAbs were isolated. Their average heavy chain (HC) SHM
134 (nucleotide level) was 6.4% (range: 2.1%-10.2%) with an average HC complementarity-
135 determining region 3 (CDR-H3) length of 15 amino acids (aa) (range: 7-23) (Table S2). The rh1987
136 KC mAbs utilized HC variable genes from the IGHV3 and IGHV4 families and predominantly used
137 KC V genes from the IGKV1 family (Table S2). All of the rh1987 KC mAbs had a CDR-L3 length of 9
138 aa and their average KC SHM (nucleotide level) was 4.7% (range: 2.6%-6.0%) (Table S2). A single
139 clonal family with 4 members (RM19A) was detected among rh1987 KC mAbs with members
140 isolated from both week 22 and week 25 samples (Table S2). The rh1987 LC mAbs used HC V
141 genes from the IGHV1, IGHV3 and IGHV4 families and LC V genes mainly from the IGLV2 gene
142 family (Table S2). The rh1987 LC mAbs had an average CDR-L3 length of 10 aa (range: 9-11) with
143 an average LC SHM (nucleotide level) of 3.8% (range: 0.9%-10.6%) (Table S2). Two clonal families
144 (RM19B [2 members] and RM19C [4 members]) were identified among the rh1987 LC mAbs
145 isolated from weeks 22 and 25 (Table S2).
146 For animal rh2011, 8 KC and 9 LC mAbs were isolated. Their average HC SHM rate
147 (nucleotide level) was 6.1% (range: 3.0%-9.1%) and they had an average CDR-H3 length of 17 aa
148 (range 10-20) (Table S2). Half of the rh2011 KC mAbs belonged to the RM20E clonal family,
149 isolated from the week 53 sample. The RM20E clonal family utilized the HC V gene IGHV5-
150 ABI*01_S2502 and the KC V gene LJI.Rh_IGKV2.71 (Table S2). Overall, the rh2011 KC mAbs had
151 an average KC SHM rate (nucleotide level) of 4.1% (range: 3.0%-5.3%) and a CDR-L3 length of 9
152 aa (Table S2). Among the rh2011 LC mAbs, two clonal families (RM20A [4 members] and RM20B

153 [2 members]) were isolated from weeks 22 and 25 samples (Table S2). Overall, the rh2011 mAbs
154 had an average LC SHM rate (nucleotide level) of 4.4% (range: 2.1%-6.4%) and an average CDR
155 L3 length of 10.6 aa (range: 9-11) (Table S2).
156
157 **BG505-specific mAbs recognize multiple Env regions**
158 All 42 mAbs bound to the BG505 SOSIP.664 trimer in ELISA, but only 11 of the 25 mAbs from
159 rh1987 and 9 of the 17 from rh2011 bound the corresponding gp120 monomer (Fig S1). The mAbs
160 were tested for neutralization activity against the autologous BG505 clade A Tier 2 virus, its
161 glycan-611 knockout variant (N611A), and the heterologous SF162 clade B Tier 1A virus. Only a
162 few mAbs, 4 from rh1987 and 2 from rh2011, neutralized the BG505.T332N pseudovirus but one
163 of them, RM20F from rh2011, did so potently (Fig 1C). Two mAbs from rh1987 and 4 from rh2011
164 were able to potently neutralize the N611A-variant despite lacking activity against the autologous
165 BG505.T332N pseudovirus (Fig 1C and D). None of the 42 mAbs neutralized the easy-to-neutralize
166 heterologous SF162 virus (Fig 1C and D).
167
168 **EM-based epitope mapping revealed mAbs isolated from both animals target 4 distinct, but**
169 **somewhat overlapping epitopes**
170 We used low resolution, negative stain, single particle electron microscopy (EM) to visualize
171 where a representative subset of the isolated mAbs bound on the surface of the BG505 SOSIP
172 trimer. The majority (55%) of mAbs isolated were non-neutralizing antibodies that bound to the
173 base of the BG505 SOSIP trimer (Figs 2A, S2, and Table S2) at a neo-epitope cluster that is
174 occluded by the viral membrane on HIV-1 virions. Fabs bound to the base of the soluble trimer

175 via multiple angles of approach and utilized a variety of heavy and light chain genes/alleles to do
176 so (Fig 2A and Table S2). The extent of SHM in the base-targeting mAbs ranged from 2-10% in the
177 HC and 1-11% in the light chain (Table S2). Previous studies examining the polyclonal antibody
178 responses elicited by the BG505 SOSIP trimers in rabbits and RMs have shown that epitopes at
179 the base of the soluble trimer were targeted in every single animal analyzed (Bianchi et al., 2018;
180 Cirelli et al., 2019; Nogal et al., 2019). Taken together with our new data, it is clear that the base
181 of SOSIP trimers contain an immunodominant non-neutralizing neo-epitope cluster that is easily
182 targeted by a variety of precursor BCRs in different species.

183 A subset of mAbs from both animals bound to an epitope near the N611 glycan (Figs 2B
184 and S2). These mAbs were not capable of neutralizing the autologous BG505.T332N pseudovirus
185 but neutralized the BG505 N611A variant (Fig 1C and D). Two additional mAbs isolated from
186 rh2011 (RM20F and RM20H) bound to an epitope near the fusion peptide (FP) and were capable
187 of neutralizing both the autologous and N611A BG505 pseudoviruses, but the latter virus more
188 potently (Figs 2C and S2). MAbs from both animals targeted the 289-glycan hole epitope on
189 BG505, with some, isolated from rh1987, showing weak neutralization of the autologous
190 BG505.T332N pseudovirus (Figs 1C and 2D; Table S2). Multiple germline genes/alleles were used
191 to target the same 289-glycan hole epitope (Table S2).

192 To further assess the epitopes targeted following immunization with the BG505
193 SOSIP.664 trimer and verify that we isolated mAbs representative of the full serum antibody
194 response, we performed electron microscopy polyclonal epitope mapping (EMPEM) (Bianchi et
195 al., 2018) using week 28 serum. EMPEM revealed that similar epitopes were targeted in both

196 animals and that the epitope assignments correlated well with the epitopes ascribed to mAbs
197 generated by antigen-specific B-cell sorting (Fig 2E versus S2).
198 A previous analysis of purified serum IgGs from RMs rh1987 and rh2011 identified the
199 C3/V5 epitope as a major target for neutralization activity (Klasse et al., 2018); however, none of
200 the mAbs isolated here targeted the C3/V5 epitope nor were they detected by EMPEM. While
201 low resolution, negative stain EM provides valuable information on where mAbs bind on the
202 surface of HIV-1 Env, the molecular detail necessary to guide structure-based immunogen design
203 requires high-resolution structural data obtained by cryoEM and x-ray crystallography. We
204 therefore selected three Fabs (RM20J, RM20F, and RM20E1) that bound to different epitopes for
205 high-resolution structural determination.
206
207 **MAb RM20J binds to the α2 helix of gp120 and exploits a hole in the glycan shield of BG505 at**
208 **position 289**
209 We solved a 2.3 Å crystal structure of unliganded RM20J Fab and a 3.9 Å cryoEM structure
210 of RM20J Fab bound to the BG505 SOSIP Env trimer (Figs 3A and S3; Tables S4 and S5.). Together
211 these structures revealed the RM20J Fab binds to an epitope on a single gp120 protomer with
212 982 $Å^2$ of buried surface area (BSA). The CDR-H1 and CDR-H2 make contact with the C2 region of
213 gp120 including residues N289 and T290 (Fig 3B). A glycan at position N289 would directly clash
214 with both the CDR-H1 and CDR-H2 of RM20J (Fig 3B). CDR-L2 makes contact with the first N-
215 acetyl glucosamine sugar of the N355 glycan (Fig 3C). Additional contacts are made to the α2
216 helix of gp120 by RM20J CDR-H3 and CDR-L2 (Fig 3C). When compared to 10A, a previously
217 characterized 241/289 glycan hole targeting NAb isolated from a BG505 SOSIP.664-immunized

218 rabbit (Bianchi et al., 2018; McCoy et al., 2016), RM20J binds to an epitope biased more towards
219 289 and away from 241 in the 241/289 glycan hole, revealing subtle differences in the recognition
220 of the epitope (Figs 3D and 3E). Despite binding to the BG505 SOSIP trimer with high affinity
221 (Table S3), RM20J was not able to neutralize the autologous BG505.T332N pseudovirus (Fig 1C).
222 Although the hypervariable region of V4 was not resolved in the trimer structure, it lies directly
223 above the RM20J epitope and contains two additional glycans (N406 and N411) that may affect
224 RM20J binding. Comparisons between the glycosylation profiles of the BG505 viral Env and the
225 SOSIP.664 trimer revealed differences in the glycoforms present at positions N355, N406, and
226 N411 (Cao et al., 2018; Struwe et al., 2018) with more complex glycans being found on the viral
227 Env that could hinder the ability of RM20J to bind on the surface of the virus and, therefore,
228 render it incapable of neutralization. Several of the mAbs isolated from rh1987, including the
229 RM19A clonal family, bind to a similar epitope as RM20J (Fig 2D, Fig S2, Table S2) and either fail
230 to neutralize the autologous BG505 virus or do so with weak potency (Fig 1C and D).
231

232 **MAb RM20F binds to a quaternary epitope at the gp120/gp41 interface that includes elements**
233 **of the fusion peptide and the N88 glycan**

234 For a more detailed view of the mode of RM20F recognition, we solved a 2.2 Å crystal
235 structure of unliganded RM20F Fab and a 4.3 Å cryoEM structure of RM20F Fab bound to BG505
236 SOSIP trimer (Figs 4A and S3; Tables S4 and S5). RM20F recognizes an epitope spanning two gp41
237 protomers and a single gp120 protomer that has 1126 Å^2 of BSA at the interface. The RM20F LC
238 contributes 22% of the paratope surface area (250 Å^2) and makes contact with the poorly
239 conserved residues H85 (8.1% prevalence among global strains) and K229 (12.5% prevalence) in

240 the C1 and C2 regions of gp120 respectively (Fig 4B). The RM20F HC contributes the remaining
241 78% of the paratope surface area (876 Å²) and uses its 20 residue CDR-H3 to wedge between the
242 FP of the primary gp41 protomer and the HR2 helix of the adjacent gp41 protomer (Fig 4C).
243 Additional contacts with the fusion peptide proximal region (FPPR) of the primary gp41 protomer
244 are made by residues at the tip of CDR-H2 (Fig 4B). The N88 glycan accounts for 18% (198 Å²) of
245 the epitope BSA and makes contact with the CDR-H2 and FR-H3 regions of RM20F (Fig 4B). The
246 lack of connecting density, even at lower contour, between RM20F and the glycans at N611 and
247 N637 suggests these glycans do not substantially contribute to the epitope. Epitope mapping
248 using BG505.T332N mutant pseudoviruses showed that knocking out the N611 glycan (N611Q
249 mutant) substantially enhanced neutralization by RM20F, while knocking out the N637 glycan
250 (N637Q mutant) had no effect. (Fig 4D). Other virus mutants revealed that neutralization by
251 RM20F was sensitive to various sequence changes within the epitope, particularly at residues
252 H85 and E647 (84.3% prevalence) and N88 (N88 glycan knock out) (Fig 4D). The N88 glycan knock
253 out and the H85A mutation (to a lesser extent) significantly reduced neutralization activity of the
254 FP-targeting bNAb VRC34, but no effect on the CD4 binding site targeting bNAb VRC01 (Fig 4D).
255 Introducing the 241 or 289 glycans (S241N and P291T, respectively) modestly reduced the
256 neutralization activity of RM20F (Fig 4D). In comparison to the FP-targeting bNAbs VRC34 and
257 ACS202, RM20F lacked neutralization breadth when tested against a panel that included multiple
258 heterologous viruses (Fig S4) likely due to the dependency on poorly conserved residues.
259
260 **MAb RM20E1 binds to the fusion peptide and makes contact with two adjacent protomers**

261 We solved a 2.3 Å crystal structure of the unliganded RM20E1 Fab and 4.4 Å cryoEM
262 structure of RM20E1 Fab bound to BG505 SOSIP trimer and Fab PGT122 (Figs 5A and S3; Tables
263 S4 and S5). RM20E1 binds to an epitope composed of one gp120 and two gp41 protomers with
264 1178 $Å^2$ of BSA. Residues 515 to 520 of the FP in the primary gp41 protomer are sandwiched
265 between CDR-H3, CDR-L1, and CDR-L3 of RM20E1 (Fig 5B). CDR-H3 and FR-H1 make contact with
266 HR2 in the adjacent gp41 protomer (Fig 5C). Additionally, the FR-H1 makes contact near the
267 N611-glycan site in the adjacent gp41 protomer, but we observed no connecting density that
268 could be attributed to the N611-glycan itself (Fig 5C). RM20E1 avoids the N88 glycan but does
269 interact with residues in the C1 region of gp120, including H85, via its CDR-L1 (Fig 5B). Despite
270 recognition of the conserved FP, RM20E1 did not neutralize the autologous BG505.T332N
271 pseudovirus. The antibody did however potently neutralize the N611A glycan KO BG505
272 pseudovirus (Fig 1C) suggesting the epitope is shielded by the N611 glycan. The epitopes of the
273 FP-targeting bNAbs VRC34, ACS202, and DFPH-a.15 overlap to a large extent with the epitopes
274 of RM20E1 and RM20F (Fig 5D), with DFPH-a.15 and VRC34 also neutralizing more potently in
275 the absence of the N611 glycan (Kong et al., 2019; Kong et al., 2016; van Gils et al., 2016; Yuan et
276 al., 2019). The RM20E1-bound FP conformation is similar to the FP conformation when bound by
277 the bNAb VRC34 (Fig S5); however, the inability of RM20E1 to accommodate the N611 glycan
278 likely results in the lack of neutralization of the wild-type virus.
279
280 **Discussion**
281 A major goal of HIV-1 vaccine research is to elicit bNAbs able to neutralize the large
282 diversity of circulating HIV-1 strains in humans. However, how to achieve this goal remains a

283 critical problem. Native-like Env trimers are an important design platform for engineering
284 immunogens for bNAb induction (de Taeye et al., 2015; Dubrovskaya et al., 2019; Escolano et al.,
285 2019; Escolano et al., 2016; Kong et al., 2019; Sanders et al., 2013; Steichen et al., 2016; Torrents
286 de la Pena et al., 2017; Yang et al., 2018). BG505 SOSIP trimers were able to induce responses in
287 immunized RMs that potently neutralized the autologous Tier 2 virus (Pauthner et al., 2017;
288 Sanders et al., 2015). When present at sufficient titers, those NAbs protected against BG505-SHIV
289 challenge (Pauthner et al., 2019). Evaluating SOSIP trimers in RMs can yield valuable information
290 because of the close genetic relationship between RMs and humans. Here, we isolated mAbs
291 from two BG505 SOSIP.664 trimer-immunized RMs to better understand how the immune
292 system recognizes the trimers and the epitopes associated with the potent, but limited, HIV-1
293 Tier 2 neutralization.

294 By mapping the epitopes of all of the mAbs isolated from the immunized RMs, rather than
295 focusing only on NAbs, we were able to identify several non-neutralizing and potentially
296 immunodominant epitopes that would ideally be eliminated in future immunization studies. As
297 shown previously with mAbs from rabbits immunized with BG505 SOSIP.664 trimers (McCoy et
298 al., 2016), the lack of glycans at positions 241 and 289 in BG505 creates a large glycan hole which
299 is targeted by mAbs from both RMs. The mAbs isolated from RMs that target the 241/289 glycan
300 hole are more biased towards the 289-site compared to the previously characterized rabbit
301 mAbs. This difference may be attributed to the underlying differences in BCR repertoires
302 between the two animal models. In addition to the lack of glycans due to missing sequons that
303 encode for glycosylation, the recombinant BG505 SOSIP.664 trimer may also contain missing
304 glycans even when the correct sequon is present as previously observed by mass spectrometry

305 studies of glycopeptides (Cao et al., 2017; Cao et al., 2018). Our study identified gp120/gp41
306 interface antibodies whose neutralization was enhanced in the absence of the N611 glycan,
307 suggesting that the BG505 SOSIP.664 trimer may have sub-stoichiometric glycan occupancy in
308 gp41 at this position, creating an unexpected but immunogenic glycan hole. The elicitation of FP
309 targeting mAbs in RMs with the BG505 SOSIP.664 trimer provides evidence that the FP bNAb
310 epitope is accessible and immunogenic on soluble Env trimer immunogens. Recent studies in
311 mice, guinea pigs and RMs using synthetically produced HIV fusion peptides covalently attached
312 to carrier proteins as priming immunogens followed by boosts with soluble Env trimer
313 immunogens have also elicited FP specific antibodies including some mAbs with neutralization
314 breadth (Cheng et al., 2019; Kong et al., 2019; Xu et al., 2018). However, the majority of the
315 animals immunized in these studies do not develop neutralization breadth and instead develop
316 potent neutralization against the BG505 pseudovirus with the N611 glycan KO (Cheng et al., 2019;
317 Kong et al., 2019; Xu et al., 2018). Given the consistency across studies and animal models in
318 eliciting potent NAbs that target the FP epitope and require the absence of the N611 glycan,
319 investing in strategies to quantify and enhance the N611 glycan occupancy in soluble Env trimer
320 immunogens, particularly for boost immunogens, may improve the neutralization breadth
321 elicited by FP-targeting immunization protocols.

322 The sorting probe used to isolate BG505 Env-specific B-cells was a C-terminally
323 biotinylated BG505 SOSIP.664 trimer bound to a fluorescent streptavidin tetramer. Steric
324 constraints between the base of the trimer and the streptavidin tetramer likely resulted in a
325 lower recovery of base epitope-specific B-cells. Despite this potential selection bias, 55% of the
326 mAbs isolated from the two immunized RMs bound to the base of the BG505 SOSIP.664 trimer,

327 indicating the base of the soluble trimer is the major target for antibody responses during
328 immunization. To reduce the immunogenicity of this epitope, glycans can be introduced to shield
329 this site or the native-like trimers could be constructed onto scaffolds or particles (Brouwer et
330 al., 2019; Georgiev et al., 2018; Kulp et al., 2017; Ringe et al., 2019).

331 We were unable to construct individual germline BCR databases from RMs rh1987 and
332 rh2011 to precisely determine the SHM and gene/alleles usage as samples of naïve PBMC
333 samples were no longer available. Instead, we constructed a germline database containing BCR
334 gene/alleles from multiple Indian origin RMs that allowed us to measure SHM levels in the mAbs
335 we isolated from RMs. The new database provides web-based access
336 (http://ward.scripps.edu/gld/) to a curated and highly annotated general resource for examining
337 BCR gene/alleles from Indian origin RMs. Previous estimates of average SHM rates in mAb
338 sequences from Env-immunized RMs were 8.9% and 6.1% for the HC and LC, respectively (Wang
339 et al., 2017). These apparently high levels of SHM following repeated immunization with the
340 exact same soluble Env immunogens were likely due to missing germline gene/alleles from the
341 database used to calculated SHM. Using the germline database reported in this study, we were
342 able to assign vaccine-elicited antibody sequences to specific germline genes/alleles and
343 determine levels of SHM much more accurately. The average levels of SHM reported in this study
344 (6.3% for HC and 4.2% for LC) are comparable to the average levels of SHM reported in similar
345 immunization studies where per animal germline BCR databases were inferred using IgDiscover
346 (Martinez-Murillo et al., 2017; Phad et al., 2020). Our germline database provides a resource for
347 assigning germline genes/alleles and accurately calculating rates of SHM when inferring
348 individual germline databases for each animal is logistically impractical.

349 In conclusion, in this study, neutralizing and non-neutralizing mAbs with distinctive
350 epitopes were isolated and characterized in BG505 SOSIP.664-immunized RMs. We
351 demonstrated that a polyclonal response was elicited in two different RMs that target the BG505
352 SOSIP.664 trimer in highly similar ways. While rabbit antibody responses are dominated by the
353 base and 241-glycan hole epitopes, the RM mAbs target more diverse epitopes with mAbs also
354 targeting the FP and gp120/gp41 interface. The mAbs characterized here also provide a valuable
355 resource for epitope mapping and comparison to a wide array of BG505-based immunization
356 experiments, including the recently initiated BG505 SOSIP.664 human clinical trial
357 (NCT03699241). Finally, the FP-targeting mAbs in particular provide a structure-guided
358 opportunity to modify BG505 SOSIP and other trimers to focus the antibody response on the FP-
359 region, with the goal of eliciting bNAb-like antibodies.
360

361 **Methods**

362 **Immunizations of rhesus macaques**

363 Immunization samples used in this study were obtained from previously immunized RMs
364 described in Sanders et al. 2015 (Sanders et al., 2015). Briefly, RMs were immunized
365 intramuscularly (i.m.) with 100 µg of BG505 SOSIP.664 trimer formulated in 75 units of
366 ISCOMATRIX given at week 0, 4, 12, 24, 38 and 52. All immunizations and blood samplings were
367 performed at the Wisconsin National Primate Research Center as described previously (Sanders
368 et al., 2015).

369 **Rhesus macaque naïve B-cell repertoire sequencing**

370 Frozen PBMCs from five naïve Indian origin RMs were obtained from Yerkes National Primate
371 Research Center (IACUC approval YER2001036). The cells were rapidly thawed in a 37°C water
372 bath and immediately diluted into 10 mL of pre-warmed RPMI media with 10% (v/v) heat-
373 inactivated fetal bovine serum (FBS). Cells were pelleted at 400xg for 7 minutes and resuspended
374 in 0.5 mL FACS buffer (PBS + 1% (v/v) FBS and stained on ice for 1 hr with the panel of fluorescent
375 antibodies against IgM ([clone G20-127] BD), CD4 ([clone OKT-4] BioLegend), CD3 ([clone SP34-
376 2] BD), IgG ([clone G18-145] BD), CD20 ([clone 2H7] BioLegend), CD8 ([clone RPA-T8] BioLegend),
377 CD14 ([clone M5E2] BD), CD16 ([clone eBioCB16] ThermoFisher) and an eFluor780 viability
378 marker (ThermoFisher). A MoFlo Astrios cell sorter (Beckman Coulter), with gating for live
379 $IgM^+/CD20^+/CD3^-/CD4^-/CD8^-/CD14^-/CD16^-$ cells, was used to isolate cells that were then pelleted
380 at 600xg for 10 min, resuspended in RLT+BME buffer (Qiagen), snap frozen in a dry ice ethanol
381 bath and stored at -80°C. RNA extraction was performed using RNeasy Protect Mini kit (Qiagen)
382 following the manufacturer's instructions. The 5' rapid amplification of cDNA ends (5'RACE) with
383 template switching method was used to obtain cDNA with unique molecular identifiers (UMIs)
384 using a protocol modified from Turchaninova *et al.* (Turchaninova et al., 2016). Briefly, 300 ng of
385 RNA was used in a 5'RACE cDNA synthesis reaction. The first-strand cDNA synthesis was
386 performed at 42°C for 1 hr using the RM IgM outer reverse primer (5'-
387 GTGATGGAGTCGGGAAGGAAG-3'), a template switch adaptor with incorporated UMIs (5'-
388 AAGCAGUGGTAUCAACGCAGAGUNNNNUNNNNUNNNNUCTTrGrGrGrG-3'), and SMARTScribe
389 Reverse Transcriptase (Clontech). Residual template switch adaptor was removed by incubation
390 with 5 U of uracil DNA glycosylase (New England BioLabs) for 40 min at 37°C. The resulting cDNA
391 was purified using the MinElute PCR Purification Kit (Qiagen) following the manufacturer's

392 instructions. PCR amplification was performed using the Q5® High-Fidelity DNA Polymerase (New
393 England BioLabs), the forward primer (5'-NNNNAAGCAGTGGTATCAACGCA-3'), and the RM IgM
394 inner reverse primer (5'-NNNNNAGGGGGAAAAGGGTTG-3'). Illumina adaptors were added using
395 the NEBNext® Ultra™ II DNA Library Prep Kit (New England BioLabs) following the manufacturer's
396 instructions. Libraries were sequenced on an Illumina MiSeq using the Illumina v3, (2x 300 bp)
397 sequencing kit.

398 **Indian origin RM germline BCR database**

399 Gene/alleles published by Vigdorovich *et al*. (Vigdorovich et al., 2016) were aligned to the
400 Mmul_8.0.1 Indian origin RM genome assembly using BLAST (Johnson et al., 2008; Zimin et al.,
401 2014). Sequences that were not identical to the reference genome were eliminated. Additional
402 full-length genes/alleles from available Indian origin RM genomic DNA sequencing datasets
403 (Cirelli et al., 2019; Ramesh et al., 2017) were added to the database. Duplicates and sequences
404 containing ambiguous bases were removed. The resulting initial Indian origin RM germline BCR
405 database (Table S1) was used for running IgDiscover on additional NGS datasets that were
406 obtained during this study as described above, downloaded from the NCBI SRA (Corcoran et al.,
407 2016; Guo et al., 2015), or obtained directly from the study authors (Vigdorovich et al., 2016).
408 Paired sequence reads were aligned and filtered for length and quality using VDJServer (Christley
409 et al., 2018). Novel germline BCR gene/alleles were inferred using IgDiscover v0.11 with the
410 germline_filter parameters "unique_cdr3s" and "unique_js" set to 10 and 4 respectively to
411 reduce the rate of false positives (Corcoran et al., 2016). Inferred genes/alleles were kept if they
412 were detected in more than one animal or if they were identical to RM genes/alleles that were
413 previously deposited in NCBI. The resulting germline BCR database (available at

414 http://ward.scripps.edu/gld/) was converted into a custom IgBLAST database and subsequently
415 used to analyze the BG505-specific mAb sequences (Ye et al., 2013).

416 **Env sequence analysis**

417 Prevalence of specific amino acids or potential N-linked glycosylation sites (PNGS) were
418 calculated using HIVAnchor (https://github.com/chazbot72/anchor). Pairwise alignments
419 between the HxB2 Env reference sequence (K03455) and the LANL 2018 Group M super filtered
420 web alignment was performed using Clustal Omega (Sievers and Higgins, 2018). The results were
421 parsed into a database keyed on positions relative to the reference, with gaps notated as sub
422 positions following the last identical residue. The database was subsequently interrogated for
423 conservation of amino acids or PNGS at specific positions.

424 **Env protein production**

425 BG505 SOSIP.664, BG505 SOSIP.664-D7324 tag, BG505 SOSIP.664-AviTag, BG505 SOSIP.v4.1, and
426 BG505 SOSIP.v5.2 were expressed in HEK293F cells and purified with either PGT145 or 2G12
427 affinity chromatograph followed by size exclusion chromatography (SEC) using a HiLoad® 16/600
428 Superdex® pg200 (GE Healthcare) as described previously (de Taeye et al., 2015; Sanders et al.,
429 2013; Torrents de la Pena et al., 2017). Monomeric gp120 proteins (AviTag or D7324 tagged)
430 were purified using a *Galanthus nivalis* lectin (Vector Labs) column. The Avi-tagged proteins were
431 biotinylated using the BirA enzyme (Avidity) according to the manufacturer's protocol. The
432 resulting biotinylated proteins are referred to using the descriptor AviB.

433 **Monoclonal antibody isolation**

434 BG505 SOSIP.664-specific IgG^+ memory B-cells from isolated PBMCs from RMs rh1987 and
435 rh2011 were single cell sorted in lysis buffer in order to amplify the antigen-specific mAbs, as

436 previously described (Sok et al., 2014). PBMCs were stained with primary fluorophore-conjugated
437 antibodies to human CD3, CD8, CD14, CD20, IgG and IgM (BD Pharmigen). For staining with Env
438 proteins, 50 nM of BG505 SOSIP.664-AviB, BG505 SOSIP.664 7C3-AviB or gp120-AviB were
439 coupled in equimolar ratios to Streptavidin-PE, Streptavidin-FITC or Streptavidin-APC (Life
440 Technologies), respectively. Cells were stained for 1 hr at 4°C in PBS supplemented with 1 mM
441 EDTA and 1% FBS. In the gating strategy, we first excluded unwanted cell populations ($CD3^-/CD8^-$
442 $/CD14^-$) followed by selection of HIV Env-specific (positive for any of the 3 probes) memory B-
443 cells ($CD20^+/IgG^+/IgM^-/HIV^+$). Cells of interest were single-cell sorted using a BD FACSAria III
444 machine, into 96-well plates containing lysis buffer, and immediately stored at -80°C. One round
445 of reverse-transcription and two rounds of nested PCR were performed to amplify the antibody
446 V(D)J genes as previously described by Tiller *et al.*[15]. The PCR products containing the variable
447 regions of the heavy chain or light chain, kappa or lambda were cloned into human IgG expression
448 vectors to produce mAbs as described previously (Sok et al., 2014). Fab expression vectors were
449 made by introducing two stop codons following residue D234 (Kabat numbering (Kabat, 1991))
450 in the IgG heavy chain vectors using the QuikChange® Lightning Site-Directed Mutagenesis kit
451 (Agilent). Sequences were verified by Sanger sequencing (Genewiz).

452 **Monoclonal antibody and Fab production**

453 MAbs and Fabs were expressed in HEK293F cells and purified using affinity chromatography.
454 Briefly, HEK293F cells (Invitrogen) were co-transfected with heavy and light chain plasmids (1:1
455 ratio) using PEImax. Transfections were performed according to the manufacturer's protocol.
456 Supernatants were harvested 4-6 days following transfection and passed through a 0.45 µm filter.
457 MAbs were purified using Protein A/G (ThermoFisher) or MAbSelect™ (GE Healthcare) affinity

458 chromatography. Fabs were purified using CaptureSelect™ CH1-XL (ThermoFisher) affinity
459 chromatography.

460 **D7324-capture ELISA for monomeric and trimeric BG505 Env proteins**

461 Binding ELISAs were conducted as described previously (Sanders et al., 2013; van Gils et al., 2016).

462 **TZM-bl cell-based neutralization assays**

463 Neutralization assays using the autologous BG505.T332N virus and mutants, and the
464 heterologous SF162 virus, were carried out as described previously (Derking et al., 2015).
465 Nonlinear regression curves were determined and 50% inhibitory concentration (IC_{50}) values
466 were calculated using a sigmoid function in Graphpad Prism v7.03.

467 **Bio-Layer Interferometry (BLI)**

468 An Octet RED instrument (FortéBio) was used to determine the kinetic parameters of the
469 antibody–antigen interactions by Biolayer Interferometry. Monoclonal Fabs were loaded onto
470 anti-human Fab-CH1 (FAB2G) biosensors (FortéBio) at a concentration of 10 µg/mL in kinetics
471 buffer (PBS, pH 7.4, 0.01% [w/v] BSA, and 0.002% [v/v] Tween 20) until a response of 1 nanometer
472 shift was reached. Loaded biosensors were dipped into kinetics buffer for 1 min to acquire a
473 baseline and then moved to wells containing a series of 2-fold dilutions of BG505 SOSIP.v5.2 in
474 kinetics buffer, starting at a 4000 nM. The trimers were allowed to associate for 180 secs before
475 the biosensor were move back to the wells containing kinetics buffer where the baseline was
476 acquired. Disassociation of the trimers from the Fab-loaded biosensors was recorded for 300
477 secs. All BLI experiments were conducted at 37°C. Kinetic parameters were calculated using the
478 Octet System Data Analysis v9.0 (FortéBio).

479 **Negative Stain Electron Microscopy**

480 BG505 SOSIP/Fab complexes were made by mixing 10-15 µg SOSIP with a 3 to 6-fold per protomer
481 molar excess for monoclonal Fabs or 500 µg polyclonal Fabs and allowed to incubate for 18 to 24
482 hrs at room temperature (RT). Complex samples were either diluted to 0.02 mg/mL and applied
483 to glow discharged negative stain grids or they were SEC purified using a Superose™ 6 Increase
484 10/300 GL (GE Healthcare) column to remove excess Fab prior to EM grid preparation. Fractions
485 containing the SOSIP/Fab complexes were pooled and concentrated using 10 kDa Amicon® spin
486 concentrators (Millipore). Samples were diluted to 0.03 mg/mL in TBS (0.05 M Tris pH 7.4, 0.15
487 M NaCl) and adsorbed onto glow discharged carbon-coated Cu400 EM grids (Electron Microscopy
488 Sciences) and blotted after 10 seconds. The grids were then stained with 3 µL of 2% (w/v) uranyl
489 formate, immediately blotted, and stained again for 45 secs followed by a final blot. Image
490 collection and data processing was performed as described previously on either an FEI Tecnai T12
491 microscope (2.05 Å/pixel; 52,000× magnification) or FEI Talos microscope (1.98 Å/pixel; 72,000×
492 magnification) with an electron dose of ~25 electrons/Å^2 using Leginon (Pugach et al., 2015;
493 Suloway et al., 2005). 2D classification, 3D sorting and 3D refinement conducted using Relion v3.0
494 (Zivanov et al., 2018). EM density maps were visualized using UCSF Chimera and segmented using
495 Segger (Pettersen et al., 2004; Pintilie et al., 2010).

496 **X-ray Crystallography Data Collection and Processing**

497 All crystals were grown using sitting drop vapor diffusion. The RM20F Fab was crystallized from
498 a solution containing 10 mg/mL protein in TBS with a well solution containing 0.1M MES, pH 5.0
499 and 2M ammonium sulfate. The crystals were cryoprotected by soaking in a well solution
500 supplemented with 30% ethylene glycol. The RM20J Fab was crystallized from a solution
501 containing 10 mg/mL protein in TBS with a well solution containing 0.1M MES, pH 6.0, 5%

502 PEG3000 and 40% PEG400, with no cryoprotectant supplemented. The RM20E1 Fab was
503 crystallized from a solution containing 6.3 mg/mL protein in TBS with a well solution containing
504 0.1M glycine, pH 10.5, 1.2M NaH_2PO_4, 0.8M Na_2HPO_4, and 0.2M Li_2SO_4, with 15% ethylene glycol
505 supplemented as cryoprotectant. All crystals were grown at 298 K. Diffraction data for RM20F
506 and RM20E1 were collected at the Stanford Synchrotron Radiation Lightsource (SSRL) beamline
507 BL12−2, and that for RM20J collected at the Advanced Photon Source (APS) beamline 23ID-B.
508 Data collection and processing statistics are detailed in Table S5. Data sets were indexed,
509 integrated, and scaled using the HKL-2000 package (Otwinowski and Minor, 1997). The structures
510 were solved by molecular replacement using PHASER (McCoy et al., 2007) with a homology model
511 (SWISS-MODEL; (Arnold et al., 2006; Biasini et al., 2014; Bordoli et al., 2009)) as a search model
512 and further refined using phenix.refine (Adams et al., 2010) combined with manual building
513 cycles in Coot (Emsley et al., 2010).

514 **Cryo Electron Microscopy Sample Preparation**

515 RM20J complex: 500 µg BG505 SOSIP.v5.2 was mixed with 656 µg RM20J Fab and incubated at
516 RT overnight. The complex was SEC purified using a HiLoad® 16/600 Superdex® pg200 (GE
517 Healthcare) column in TBS. Fractions containing the complex were concentrated to 6.1 mg/mL
518 using a 10 kDa Amicon® spin concentrator (Millipore). 3.5 µL of the complex was mixed with 0.57
519 µL of 0.04 mM lauryl maltose neopentyl glycol (LMNG) and applied to a C-Flat grid (CF-2/1-4C,
520 Protochips, Inc.), which had been plasma-cleaned for 5 seconds using a mixture of N_2/O_2 (Gatan
521 Solarus 950 Plasma system). The grid was blotted and plunged into liquid ethane using a Vitrobot
522 Mark IV (ThermoFisher).

523 RM20F complex: 500 µg BG505 SOSIP.v4.1 was mixed with approximately 1,000 µg RM20F Fab
524 and incubated at RT overnight. The complex was SEC purified using a Superose™ 6 Increase
525 10/300 GL (GE Healthcare) column in TBS. Fractions containing the complex were concentrated
526 to 6 mg/mL using a 10 kDa Amicon® spin concentrator (Millipore). 3 µL of the complex was mixed
527 with 1 µL of a n-Dodecyl-β-D-Maltopyranoside (DDM) solution to a final DDM concentration of
528 0.06 mM and applied to a C-Flat grid (CF-2/2-4C, Protochips, Inc.), which had been plasma-
529 cleaned for 5 seconds using a mixture of N_2/O_2 (Gatan Solarus 950 Plasma system). The grid was
530 blotted and plunged into liquid Ethane using a Vitrobot Mark IV (ThermoFisher).
531 RM20E1 complex: 355 µg BG505 SOSIP.v5.2 was mixed with 484 µg RM20E1 Fab and 484 µg
532 PGT122 Fab and incubated at RT overnight. The complex was SEC purified using a HiLoad® 16/600
533 Superdex® pg200 (GE Healthcare) column in TBS. Fractions containing the complex were
534 concentrated to 4 mg/mL using a 10 kDa Amicon® spin concentrator (Millipore). 3 µL of the
535 complex was mixed with 1 µL of a n-Dodecyl-β-D-Maltopyranoside (DDM) solution to a final DDM
536 concentration of 0.06 mM and applied to a grid (Quantifoil R 1.2/1.3, 400), which had been
537 plasma-cleaned for 5 seconds using a mixture of N_2/O_2 (Gatan Solarus 950 Plasma system). The
538 grid was blotted and plunged into liquid Ethane using a Vitrobot Mark IV (ThermoFisher).
539 **Cryo Electron Microscopy Data Collection and Processing**
540 Samples were imaged on either FEI Titan Krios electron microscope (ThermoFisher) operating at
541 300 keV (RM20F dataset) or a FEI Talos Arctica electron microscope (ThermoFisher) operating at
542 200 keV (RM20J and RM20E1 datasets). Both microscopes were equipped with Gatan K2 Summit
543 direct electron directors operating in counting mode. Automated data collection was performed
544 using the Leginon software suite (Suloway et al., 2005). Micrograph movie frames were aligned

545 and dose-weighted using MotionCor2 (Zheng et al., 2017), and CTF models were determined
546 using Gctf (Zhang, 2016). Particle picking, 2D classification, Ab-initio reconstruction, and 3D
547 refinement were conducted using cryoSPARCv2 (Punjani et al., 2017). Data collection and
548 processing parameters are reported in Table S4.

549 Initial molecular models of the BG505 SOSIP trimer/Fab complexes were built by docking the Env
550 portion of PDB: 5V8M (Lee et al., 2017) into the EM density maps along with the relevant Fab
551 crystal structures (PDB: 4JY5 was used for PGT122 (Julien et al., 2013b)) using UCSF Chimera
552 (Pettersen et al., 2004). The Fab constant regions were removed due to flexibility in the elbow
553 region as commonly found in Fab structures (Bailey et al., 2018), the appropriate stabilizing
554 mutations (v4.1 or v5.2) were introduced into the Env sequence, and N-linked glycans were
555 added using Coot (van Beusekom et al., 2019). The models were iteratively refined into the EM
556 density maps using RosettaRelax and Coot (Casanal et al., 2019; DiMaio et al., 2009; Emsley et
557 al., 2010; Frenz et al., 2018; van Beusekom et al., 2019). Glycan structures were validated using
558 Privateer (Agirre et al., 2015). Overall structures were evaluated using EMRinger (Barad et al.,
559 2015) and MolProbity (Williams et al., 2018). Protein interface calculations were performed using
560 jsPISA (Krissinel, 2015). Final model statistics are summarized in Table S4.

561 **Statistical analysis**

562 Statistical models inherent to Relion 3.0 (Zivanov et al., 2018) and cryoSPARC (Punjani et al.,
563 2017) were employed in image analysis to derive 2D classes and 3D models. All ELISA and
564 neutralization assays were conducted with at least duplicate measurements.

565 **Data and Software Availability**

566 The accession numbers for Env-specific BCR sequences are DDBJ/ENA/GenBank: MT002976-
567 MT002992 and MT008262-MT008328. RM IgM BCR sequences are available under BioProject ID:
568 PRJNA604386. Atomic coordinates and structure factors of the reported crystal structure have
569 been deposited in the Protein Data Bank (PDB: 6VOS, 6VOR). Cryo-EM reconstructions have been
570 deposited in the Electron Microscopy Data Bank (EMDB: EMD-21246, EMD-21257, EMD-21232),
571 and in the Protein Data Bank (PDB: 6VN0, 6VO1, 6VLR). The accession numbers for the negative
572 stain 3D EM reconstructions are Electron Microscopy DataBank: EMD-21053, EMD-21055, EMD-
573 21056, EMD-21057, EMD-21058, EMD-21059, EMD-21061, EMD-21062, EMD-21064, EMD-
574 21065, EMD-21066, EMD-21075, EMD-21076, EMD-21077, EMD-21078, EMD-21079, EMD-
575 21080, EMD-21081, EMD-21082, EMD-21083, EMD-21084, EMD-21085, EMD-21086, EMD-
576 21087, EMD-21088, EMD-21089, EMD-21090, EMD-21091, EMD-21092, EMD-21093, EMD-
577 21272, EMD-21273, EMD-21274, EMD-21275, EMD-21276, EMD-21277, EMD-21278.
578
579 **Figure Legends**
580 **Figure 1.** MAb isolation and characterization from BG505 SOSIP.664 trimer-immunized RMs. (A)
581 Simplified immunization scheme adapted from Sanders et al. 2015 (Sanders et al., 2015). Black
582 arrows indicate i.m. immunizations with 100 µg of BG505 SOSIP.664 with 75 units of ISCOMATRIX
583 adjuvant. Red arrows indicate blood draws. (B) Heavy and light chain genetic characteristics for
584 mAbs isolated from rh1987 and rh2011. (C) TZM-bl neutralization of BG505.T332N,
585 BG505.T332N.N611A, and SF162 pseudoviruses for mAbs isolated from RM rh1987. (D) TZM-bl
586 neutralization of BG505.T332N, BG505.T332N.N611A, and SF162 pseudoviruses for mAbs
587 isolated from RM rh2011. Assay limit of detection was at an IC_{50} of 50 µg/mL.

588 **Figure 2.** Epitope mapping by negative stain electron microscopy. (A) Representative base-
589 targeting mAbs for animals rh1987 and rh2011. (B) Overlapping gp120/gp41 interface epitope
590 targeted by mAbs from both animals. (C) Overlapping FP epitope targeted by mAbs from both
591 animals. (D) Overlapping N289-glycan hole epitope targeted by mAbs from both animals. (E)
592 EMPEM analysis for wk28 IgG from rh2011 and rh1987. All structural figures were generated with
593 UCSF Chimera (Pettersen et al., 2004). EM density maps were segmented with the Segger
594 extension in UCSF Chimera (Pettersen et al., 2004; Pintilie et al., 2010).

595 **Figure 3.** RM20J binds to the N289 glycan hole region of BG505 SOSIP.v5.2 (A) Segmented 3.9 Å
596 cryoEM reconstruction of RM20J Fab (pink) in complex with BG505 SOSIP.v5.2 (gp120, dark blue;
597 gp41, light blue). (B) and (C) Zoomed-in views of the epitope/paratope interaction between
598 gp120 (blue, ribbon diagram) and RM20J Fab (surface representation). (D) and (E) Comparison of
599 the RM20J epitope with that of the BG505 SOSIP.664 elicited rabbit neutralizing NAb 10A (PDB:
600 6DID) (Bianchi et al., 2018; McCoy et al., 2016).

601 **Figure 4.** RM20F binds to a quaternary epitope at the gp120/gp41 interface of BG505 SOSIP.v4.1.
602 (A) Segmented 4.3 Å cryoEM reconstruction of RM20F Fab (orange) in complex with BG505 SOSIP
603 (gp120, dark blue; gp41, light blue). (B) and (C) Zoomed-in views of the epitope/paratope
604 interaction between BG505 SOSIP (gp120, dark blue; gp41s, light blue and light green; ribbon
605 diagram) and RM20F Fab (surface representation). (D) Neutralization data for BG505 mutant
606 pseudoviruses against VRC01, RM20F, and VRC34.

607 **Figure 5.** RM20E1 binds to the fusion peptide of BG505 SOSIP.v5.2. (A) Segmented 4.2 Å cryoEM
608 reconstruction of RM20E1 Fab (yellow) and PGT122 Fab (light green) in complex with BG505
609 SOSIP (gp120, dark blue; gp41, light blue). (B) and (C) Zoomed-in views of the epitope/paratope

610 interaction between BG505 SOSIP (gp120, dark blue; gp41s, light blue and light green; ribbon
611 diagram) and RM20E1 Fab (surface representation). (D) Comparison of RM20E1 and RM20F
612 epitopes to those of FP targeting bNAbs VRC34, ACS202, and DFPH-a.15 (Kong et al., 2019; Kong
613 et al., 2016; van Gils et al., 2016; Yuan et al., 2019).

614 **Table S1.** Initial germline BCR database used in IgDiscover

615

616 **Acknowledgements**

617 We thank Jean-Christophe Ducom, Hannah Turner, and Bill Anderson for assistance with
618 computational resources, microscope management, and data collection. We thank Alan Saluk,
619 Brian Seegers, Steven Head, Jessica Ledesma, Curt Wittenberg, and Nitya Bhaskaran for
620 assistance with naïve B-cell sorting and NGS sequencing. This work was supported by the HIV
621 Vaccine Research and Design (HIVRAD) program (P01 AI110657) (A.B.W., R.W.S, J.P.M., and
622 I.A.W.), NIH CHAVI-ID (UM1 AI100663) and CHAVD (UM1 AI44462) awards (A.B.W., I.A.W. and
623 D.R.B.), NIH R01 AI13082 (J.P.M.), the International AIDS Vaccine Initiative Neutralizing Antibody
624 Center, the Bill and Melinda Gates Foundation CAVD (OPP1115782, OPP1132237, OPP1084519,
625 OPP119635), and the European Union's Horizon 2020 research and innovation program under
626 grant agreement no. 681137 (R.W.S.). C.A.C. is supported by the NIH F31 Ruth L. Kirschstein
627 Predoctoral Award Al131873 and by the Achievement Rewards for College Scientists Foundation.
628 R.W.S. is a recipient of a Vici fellowship from the Netherlands Organization for Scientific Research
629 (NWO). G.O. and M.J.v.G. are supported by amfAR Mathilde Krim Fellowships in Basic Biomedical
630 Research grant numbers 109718-63-RKNT and 109514-61-RKVA, respectively. J.v.S. is a recipient
631 of a 2017 AMC Ph.D. Scholarship. Computational analyses of EM data were performed using

632 shared instrumentation funded by NIH grant S10OD021634. Naïve B-cell sorting and NGS
633 sequencing was conducted as part of the Technologies Across Scale graduate course with support
634 from Skaggs Graduate School of Chemical and Biological Sciences at Scripps Research. Use of the
635 Stanford Synchrotron Radiation Lightsource, SLAC National Accelerator Laboratory, is supported
636 by the U.S. Department of Energy, Office of Science, Office of Basic Energy Sciences under
637 Contract No. DE-AC02-76SF00515. The SSRL Structural Molecular Biology Program is supported
638 by the DOE Office of Biological and Environmental Research, and by the National Institutes of
639 Health, National Institute of General Medical Sciences (including P41GM103393). The contents
640 of this publication are solely the responsibility of the authors and do not necessarily represent
641 the official views of NIGMS, NIAID, or NIH.

642

643 **References**

644 Adams, P.D., Afonine, P.V., Bunkoczi, G., Chen, V.B., Davis, I.W., Echols, N., Headd, J.J., Hung,
645 L.W., Kapral, G.J., Grosse-Kunstleve, R.W.*, et al.* (2010). PHENIX: a comprehensive Python-based
646 system for macromolecular structure solution. Acta crystallographica Section D, Biological
647 crystallography *66*, 213-221.
648 Agirre, J., Iglesias-Fernandez, J., Rovira, C., Davies, G.J., Wilson, K.S., and Cowtan, K.D. (2015).
649 Privateer: software for the conformational validation of carbohydrate structures. Nature
650 structural & molecular biology *22*, 833-834.
651 Arnold, K., Bordoli, L., Kopp, J., and Schwede, T. (2006). The SWISS-MODEL workspace: a web-
652 based environment for protein structure homology modelling. Bioinformatics *22*, 195-201.
653 Bailey, L.J., Sheehy, K.M., Dominik, P.K., Liang, W.G., Rui, H., Clark, M., Jaskolowski, M., Kim, Y.,
654 Deneka, D., Tang, W.J.*, et al.* (2018). Locking the Elbow: Improved Antibody Fab Fragments as
655 Chaperones for Structure Determination. Journal of molecular biology *430*, 337-347.
656 Barad, B.A., Echols, N., Wang, R.Y., Cheng, Y., DiMaio, F., Adams, P.D., and Fraser, J.S. (2015).
657 EMRinger: side chain-directed model and map validation for 3D cryo-electron microscopy.
658 Nature methods *12*, 943-946.
659 Bianchi, M., Turner, H.L., Nogal, B., Cottrell, C.A., Oyen, D., Pauthner, M., Bastidas, R., Nedellec,
660 R., McCoy, L.E., Wilson, I.A.*, et al.* (2018). Electron-Microscopy-Based Epitope Mapping Defines
661 Specificities of Polyclonal Antibodies Elicited during HIV-1 BG505 Envelope Trimer
662 Immunization. Immunity *49*, 288-300 e288.

663 Biasini, M., Bienert, S., Waterhouse, A., Arnold, K., Studer, G., Schmidt, T., Kiefer, F., Gallo
664 Cassarino, T., Bertoni, M., Bordoli, L.*, et al.* (2014). SWISS-MODEL: modelling protein tertiary
665 and quaternary structure using evolutionary information. Nucleic Acids Res *42*, W252-258.
666 Bordoli, L., Kiefer, F., Arnold, K., Benkert, P., Battey, J., and Schwede, T. (2009). Protein
667 structure homology modeling using SWISS-MODEL workspace. Nature protocols *4*, 1-13.
668 Brouwer, P.J.M., Antanasijevic, A., Berndsen, Z., Yasmeen, A., Fiala, B., Bijl, T.P.L., Bontjer, I.,
669 Bale, J.B., Sheffler, W., Allen, J.D.*, et al.* (2019). Enhancing and shaping the immunogenicity of
670 native-like HIV-1 envelope trimers with a two-component protein nanoparticle. Nat Commun
671 *10*, 4272.
672 Burton, D.R., and Hangartner, L. (2016). Broadly Neutralizing Antibodies to HIV and Their Role in
673 Vaccine Design. Annual review of immunology *34*, 635-659.
674 Cao, L., Diedrich, J.K., Kulp, D.W., Pauthner, M., He, L., Park, S.R., Sok, D., Su, C.Y., Delahunty,
675 C.M., Menis, S.*, et al.* (2017). Global site-specific N-glycosylation analysis of HIV envelope
676 glycoprotein. Nat Commun *8*, 14954.
677 Cao, L., Pauthner, M., Andrabi, R., Rantalainen, K., Berndsen, Z., Diedrich, J.K., Menis, S., Sok, D.,
678 Bastidas, R., Park, S.R.*, et al.* (2018). Differential processing of HIV envelope glycans on the virus
679 and soluble recombinant trimer. Nat Commun *9*, 3693.
680 Casanal, A., Lohkamp, B., and Emsley, P. (2019). Current Developments in Coot for
681 Macromolecular Model Building of Electron Cryo-microscopy and Crystallographic Data. Protein
682 science : a publication of the Protein Society.
683 Cheng, C., Xu, K., Kong, R., Chuang, G.Y., Corrigan, A.R., Geng, H., Hill, K.R., Jafari, A.J., O'Dell, S.,
684 Ou, L.*, et al.* (2019). Consistent elicitation of cross-clade HIV-neutralizing responses achieved in
685 guinea pigs after fusion peptide priming by repetitive envelope trimer boosting. PloS one *14*,
686 e0215163.
687 Christley, S., Scarborough, W., Salinas, E., Rounds, W.H., Toby, I.T., Fonner, J.M., Levin, M.K.,
688 Kim, M., Mock, S.A., Jordan, C.*, et al.* (2018). VDJServer: A Cloud-Based Analysis Portal and Data
689 Commons for Immune Repertoire Sequences and Rearrangements. Frontiers in immunology *9*,
690 976.
691 Cirelli, K.M., Carnathan, D.G., Nogal, B., Martin, J.T., Rodriguez, O.L., Upadhyay, A.A., Enemuo,
692 C.A., Gebru, E.H., Choe, Y., Viviano, F.*, et al.* (2019). Slow Delivery Immunization Enhances HIV
693 Neutralizing Antibody and Germinal Center Responses via Modulation of Immunodominance.
694 Cell.
695 Corcoran, M.M., Phad, G.E., Nestor, V.B., Stahl-Hennig, C., Sumida, N., Persson, M.A., Martin,
696 M., and Karlsson Hedestam, G.B. (2016). Production of individualized V gene databases reveals
697 high levels of immunoglobulin genetic diversity. Nat Commun *7*, 13642.
698 de Taeye, S.W., Ozorowski, G., Torrents de la Pena, A., Guttman, M., Julien, J.P., van den
699 Kerkhof, T.L., Burger, J.A., Pritchard, L.K., Pugach, P., Yasmeen, A.*, et al.* (2015). Immunogenicity
700 of Stabilized HIV-1 Envelope Trimers with Reduced Exposure of Non-neutralizing Epitopes. Cell
701 *163*, 1702-1715.
702 Derking, R., Ozorowski, G., Sliepen, K., Yasmeen, A., Cupo, A., Torres, J.L., Julien, J.P., Lee, J.H.,
703 van Montfort, T., de Taeye, S.W.*, et al.* (2015). Comprehensive antigenic map of a cleaved
704 soluble HIV-1 envelope trimer. PLoS pathogens *11*, e1004767.

705 DiMaio, F., Tyka, M.D., Baker, M.L., Chiu, W., and Baker, D. (2009). Refinement of protein
706 structures into low-resolution density maps using rosetta. Journal of molecular biology *392*,
707 181-190.
708 Dubrovskaya, V., Tran, K., Ozorowski, G., Guenaga, J., Wilson, R., Bale, S., Cottrell, C.A., Turner,
709 H.L., Seabright, G., O'Dell, S.*, et al.* (2019). Vaccination with Glycan-Modified HIV NFL Envelope
710 Trimer-Liposomes Elicits Broadly Neutralizing Antibodies to Multiple Sites of Vulnerability.
711 Immunity *51*, 915-929 e917.
712 Emsley, P., Lohkamp, B., Scott, W.G., and Cowtan, K. (2010). Features and development of Coot.
713 Acta crystallographica Section D, Biological crystallography *66*, 486-501.
714 Escolano, A., Gristick, H.B., Abernathy, M.E., Merkenschlager, J., Gautam, R., Oliveira, T.Y., Pai,
715 J., West, A.P., Jr., Barnes, C.O., Cohen, A.A.*, et al.* (2019). Immunization expands B cells specific
716 to HIV-1 V3 glycan in mice and macaques. Nature *570*, 468-473.
717 Escolano, A., Steichen, J.M., Dosenovic, P., Kulp, D.W., Golijanin, J., Sok, D., Freund, N.T., Gitlin,
718 A.D., Oliveira, T., Araki, T.*, et al.* (2016). Sequential Immunization Elicits Broadly Neutralizing
719 Anti-HIV-1 Antibodies in Ig Knockin Mice. Cell *166*, 1445-1458 e1412.
720 Frenz, B., Ramisch, S., Borst, A.J., Walls, A.C., Adolf-Bryfogle, J., Schief, W.R., Veesler, D., and
721 DiMaio, F. (2018). Automatically Fixing Errors in Glycoprotein Structures with Rosetta.
722 Structure.
723 Gadala-Maria, D., Yaari, G., Uduman, M., and Kleinstein, S.H. (2015). Automated analysis of
724 high-throughput B-cell sequencing data reveals a high frequency of novel immunoglobulin V
725 gene segment alleles. Proceedings of the National Academy of Sciences of the United States of
726 America *112*, E862-870.
727 Georgiev, I.S., Joyce, M.G., Chen, R.E., Leung, K., McKee, K., Druz, A., Van Galen, J.G., Kanekiyo,
728 M., Tsybovsky, Y., Yang, E.S.*, et al.* (2018). Two-Component Ferritin Nanoparticles for
729 Multimerization of Diverse Trimeric Antigens. ACS Infect Dis *4*, 788-796.
730 Guo, K., Halemano, K., Schmitt, K., Katuwal, M., Wang, Y., Harper, M.S., Heilman, K.J., Kuwata,
731 T., Stephens, E.B., and Santiago, M.L. (2015). Immunoglobulin VH gene diversity and somatic
732 hypermutation during SIV infection of rhesus macaques. Immunogenetics *67*, 355-370.
733 Jardine, J.G., Kulp, D.W., Havenar-Daughton, C., Sarkar, A., Briney, B., Sok, D., Sesterhenn, F.,
734 Ereno-Orbea, J., Kalyuzhniy, O., Deresa, I.*, et al.* (2016). HIV-1 broadly neutralizing antibody
735 precursor B cells revealed by germline-targeting immunogen. Science *351*, 1458-1463.
736 Johnson, M., Zaretskaya, I., Raytselis, Y., Merezhuk, Y., McGinnis, S., and Madden, T.L. (2008).
737 NCBI BLAST: a better web interface. Nucleic Acids Res *36*, W5-9.
738 Julien, J.P., Cupo, A., Sok, D., Stanfield, R.L., Lyumkis, D., Deller, M.C., Klasse, P.J., Burton, D.R.,
739 Sanders, R.W., Moore, J.P.*, et al.* (2013a). Crystal structure of a soluble cleaved HIV-1 envelope
740 trimer. Science *342*, 1477-1483.
741 Julien, J.P., Sok, D., Khayat, R., Lee, J.H., Doores, K.J., Walker, L.M., Ramos, A., Diwanji, D.C.,
742 Pejchal, R., Cupo, A.*, et al.* (2013b). Broadly neutralizing antibody PGT121 allosterically
743 modulates CD4 binding via recognition of the HIV-1 gp120 V3 base and multiple surrounding
744 glycans. PLoS pathogens *9*, e1003342.
745 Kabat, E.A. (1991). Sequences of proteins of immunological interest : tabulation and analysis of
746 amino acid and nucleic acid sequences of precursors, V-regions, C-regions, J-chain, T-cell
747 receptors for antigenm T-cell surface antigens, [beta]2-microglobulins,major histocompatibility
748 antigens, Thy-1, complement, C-reactive protein, thymopoietin, integrins, post-gamme globulin,

749 [alpha]2-macroglobulins, and other related proteins, 5th edn (Bethesda, Md. (Bethesda,
750 20892): U.S. Dept. of Health and Human Services, Public Health Service, National Institutes of
751 Health).
752 Klasse, P.J., Ketas, T.J., Cottrell, C.A., Ozorowski, G., Debnath, G., Camara, D., Francomano, E.,
753 Pugach, P., Ringe, R.P., LaBranche, C.C.*, et al.* (2018). Epitopes for neutralizing antibodies
754 induced by HIV-1 envelope glycoprotein BG505 SOSIP trimers in rabbits and macaques. PLoS
755 pathogens *14*, e1006913.
756 Kong, R., Duan, H., Sheng, Z., Xu, K., Acharya, P., Chen, X., Cheng, C., Dingens, A.S., Gorman, J.,
757 Sastry, M.*, et al.* (2019). Antibody Lineages with Vaccine-Induced Antigen-Binding Hotspots
758 Develop Broad HIV Neutralization. Cell *178*, 567-584 e519.
759 Kong, R., Xu, K., Zhou, T., Acharya, P., Lemmin, T., Liu, K., Ozorowski, G., Soto, C., Taft, J.D.,
760 Bailer, R.T.*, et al.* (2016). Fusion peptide of HIV-1 as a site of vulnerability to neutralizing
761 antibody. Science *352*, 828-833.
762 Krissinel, E. (2015). Stock-based detection of protein oligomeric states in jsPISA. Nucleic Acids
763 Res *43*, W314-319.
764 Kulp, D.W., Steichen, J.M., Pauthner, M., Hu, X., Schiffner, T., Liguori, A., Cottrell, C.A., Havenar-
765 Daughton, C., Ozorowski, G., Georgeson, E.*, et al.* (2017). Structure-based design of native-like
766 HIV-1 envelope trimers to silence non-neutralizing epitopes and eliminate CD4 binding. Nat
767 Commun *8*, 1655.
768 Landais, E., and Moore, P.L. (2018). Development of broadly neutralizing antibodies in HIV-1
769 infected elite neutralizers. Retrovirology *15*, 61.
770 Lee, J.H., Andrabi, R., Su, C.Y., Yasmeen, A., Julien, J.P., Kong, L., Wu, N.C., McBride, R., Sok, D.,
771 Pauthner, M.*, et al.* (2017). A Broadly Neutralizing Antibody Targets the Dynamic HIV Envelope
772 Trimer Apex via a Long, Rigidified, and Anionic beta-Hairpin Structure. Immunity *46*, 690-702.
773 Lei, L., Yang, Y.R., Tran, K., Wang, Y., Chiang, C.I., Ozorowski, G., Xiao, Y., Ward, A.B., Wyatt, R.T.,
774 and Li, Y. (2019). The HIV-1 Envelope Glycoprotein C3/V4 Region Defines a Prevalent
775 Neutralization Epitope following Immunization. Cell Rep *27*, 586-598 e586.
776 Lyumkis, D., Julien, J.P., de Val, N., Cupo, A., Potter, C.S., Klasse, P.J., Burton, D.R., Sanders,
777 R.W., Moore, J.P., Carragher, B.*, et al.* (2013). Cryo-EM structure of a fully glycosylated soluble
778 cleaved HIV-1 envelope trimer. Science *342*, 1484-1490.
779 Martinez-Murillo, P., Tran, K., Guenaga, J., Lindgren, G., Adori, M., Feng, Y., Phad, G.E., Vazquez
780 Bernat, N., Bale, S., Ingale, J.*, et al.* (2017). Particulate Array of Well-Ordered HIV Clade C Env
781 Trimers Elicits Neutralizing Antibodies that Display a Unique V2 Cap Approach. Immunity *46*,
782 804-817 e807.
783 McCoy, A.J., Grosse-Kunstleve, R.W., Adams, P.D., Winn, M.D., Storoni, L.C., and Read, R.J.
784 (2007). Phaser crystallographic software. J Appl Crystallogr *40*, 658-674.
785 McCoy, L.E., van Gils, M.J., Ozorowski, G., Messmer, T., Briney, B., Voss, J.E., Kulp, D.W.,
786 Macauley, M.S., Sok, D., Pauthner, M.*, et al.* (2016). Holes in the Glycan Shield of the Native HIV
787 Envelope Are a Target of Trimer-Elicited Neutralizing Antibodies. Cell Rep *16*, 2327-2338.
788 Moldt, B., Le, K.M., Carnathan, D.G., Whitney, J.B., Schultz, N., Lewis, M.G., Borducchi, E.N.,
789 Smith, K.M., Mackel, J.J., Sweat, S.L.*, et al.* (2016). Neutralizing antibody affords comparable
790 protection against vaginal and rectal simian/human immunodeficiency virus challenge in
791 macaques. Aids *30*, 1543-1551.

792 Nogal, B., Bianchi, M., Cottrell, C.A., Kirchdoerfer, R.N., Sewall, L.M., Turner, H.L., Zhao, F., Sok,
793 D., Burton, D.R., Hangartner, L.*, et al.* (2019). Mapping polyclonal antibody responses in non-
794 human primates vaccinated with HIV Env trimer subunit vaccines. bioRxiv, 833715.
795 Otwinowski, Z., and Minor, W. (1997). Processing of X-ray diffraction data collected in
796 oscillation mode. Methods Enzymol *276*, 307-326.
797 Pancera, M., Zhou, T., Druz, A., Georgiev, I.S., Soto, C., Gorman, J., Huang, J., Acharya, P.,
798 Chuang, G.Y., Ofek, G.*, et al.* (2014). Structure and immune recognition of trimeric pre-fusion
799 HIV-1 Env. Nature *514*, 455-461.
800 Pauthner, M., Havenar-Daughton, C., Sok, D., Nkolola, J.P., Bastidas, R., Boopathy, A.V.,
801 Carnathan, D.G., Chandrashekar, A., Cirelli, K.M., Cottrell, C.A.*, et al.* (2017). Elicitation of
802 Robust Tier 2 Neutralizing Antibody Responses in Nonhuman Primates by HIV Envelope Trimer
803 Immunization Using Optimized Approaches. Immunity *46*, 1073-1088 e1076.
804 Pauthner, M.G., Nkolola, J.P., Havenar-Daughton, C., Murrell, B., Reiss, S.M., Bastidas, R.,
805 Prevost, J., Nedellec, R., von Bredow, B., Abbink, P.*, et al.* (2019). Vaccine-Induced Protection
806 from Homologous Tier 2 SHIV Challenge in Nonhuman Primates Depends on Serum-Neutralizing
807 Antibody Titers. Immunity *50*, 241-252 e246.
808 Pegu, A., Borate, B., Huang, Y.D., Pauthner, M.G., Hessell, A.J., Julg, B., Doria-Rose, N.A.,
809 Schmidt, S.D., Carpp, L.N., Cully, M.D.*, et al.* (2019). A Meta-analysis of Passive Immunization
810 Studies Shows that Serum-Neutralizing Antibody Titer Associates with Protection against SHIV
811 Challenge. Cell Host & Microbe *26*, 336-+.
812 Pettersen, E.F., Goddard, T.D., Huang, C.C., Couch, G.S., Greenblatt, D.M., Meng, E.C., and
813 Ferrin, T.E. (2004). UCSF Chimera--a visualization system for exploratory research and analysis. J
814 Comput Chem *25*, 1605-1612.
815 Phad, G.E., Pushparaj, P., Tran, K., Dubrovskaya, V., Adori, M., Martinez-Murillo, P., Vazquez
816 Bernat, N., Singh, S., Dionne, G., O'Dell, S.*, et al.* (2020). Extensive dissemination and intraclonal
817 maturation of HIV Env vaccine-induced B cell responses. The Journal of experimental medicine
818 *217*.
819 Pintilie, G.D., Zhang, J., Goddard, T.D., Chiu, W., and Gossard, D.C. (2010). Quantitative analysis
820 of cryo-EM density map segmentation by watershed and scale-space filtering, and fitting of
821 structures by alignment to regions. Journal of structural biology *170*, 427-438.
822 Pugach, P., Ozorowski, G., Cupo, A., Ringe, R., Yasmeen, A., de Val, N., Derking, R., Kim, H.J.,
823 Korzun, J., Golabek, M.*, et al.* (2015). A native-like SOSIP.664 trimer based on an HIV-1 subtype
824 B env gene. J Virol *89*, 3380-3395.
825 Punjani, A., Rubinstein, J.L., Fleet, D.J., and Brubaker, M.A. (2017). cryoSPARC: algorithms for
826 rapid unsupervised cryo-EM structure determination. Nature methods *14*, 290-296.
827 Ralph, D.K., and Matsen, F.A.I. (2018). Per-sample immunoglobulin germline inference from B
828 cell receptor deep sequencing data. arXiv.
829 Ramesh, A., Darko, S., Hua, A., Overman, G., Ransier, A., Francica, J.R., Trama, A., Tomaras, G.D.,
830 Haynes, B.F., Douek, D.C.*, et al.* (2017). Structure and Diversity of the Rhesus Macaque
831 Immunoglobulin Loci through Multiple De Novo Genome Assemblies. Frontiers in immunology
832 *8*, 1407.
833 Ringe, R.P., Cruz Portillo, V.M., Dosenovic, P., Ketas, T.J., Ozorowski, G., Nogal, B., Perez, L.,
834 LaBranche, C.C., Lim, J., Francomano, E.*, et al.* (2019). Neutralizing antibody induction by HIV-1

835 Envelope glycoprotein SOSIP trimers on iron oxide nanoparticles may be impaired by mannose
836 binding lectin. J Virol.
837 Sanders, R.W., Derking, R., Cupo, A., Julien, J.P., Yasmeen, A., de Val, N., Kim, H.J., Blattner, C.,
838 de la Pena, A.T., Korzun, J.*, et al.* (2013). A next-generation cleaved, soluble HIV-1 Env trimer,
839 BG505 SOSIP.664 gp140, expresses multiple epitopes for broadly neutralizing but not non-
840 neutralizing antibodies. PLoS pathogens *9*, e1003618.
841 Sanders, R.W., van Gils, M.J., Derking, R., Sok, D., Ketas, T.J., Burger, J.A., Ozorowski, G., Cupo,
842 A., Simonich, C., Goo, L.*, et al.* (2015). HIV-1 VACCINES. HIV-1 neutralizing antibodies induced by
843 native-like envelope trimers. Science *349*, aac4223.
844 Sievers, F., and Higgins, D.G. (2018). Clustal Omega for making accurate alignments of many
845 protein sequences. Protein science : a publication of the Protein Society *27*, 135-145.
846 Sok, D., van Gils, M.J., Pauthner, M., Julien, J.P., Saye-Francisco, K.L., Hsueh, J., Briney, B., Lee,
847 J.H., Le, K.M., Lee, P.S.*, et al.* (2014). Recombinant HIV envelope trimer selects for quaternary-
848 dependent antibodies targeting the trimer apex. Proceedings of the National Academy of
849 Sciences of the United States of America *111*, 17624-17629.
850 Steichen, J.M., Kulp, D.W., Tokatlian, T., Escolano, A., Dosenovic, P., Stanfield, R.L., McCoy, L.E.,
851 Ozorowski, G., Hu, X., Kalyuzhniy, O.*, et al.* (2016). HIV Vaccine Design to Target Germline
852 Precursors of Glycan-Dependent Broadly Neutralizing Antibodies. Immunity *45*, 483-496.
853 Struwe, W.B., Chertova, E., Allen, J.D., Seabright, G.E., Watanabe, Y., Harvey, D.J., Medina-
854 Ramirez, M., Roser, J.D., Smith, R., Westcott, D.*, et al.* (2018). Site-Specific Glycosylation of
855 Virion-Derived HIV-1 Env Is Mimicked by a Soluble Trimeric Immunogen. Cell Rep *24*, 1958-1966
856 e1955.
857 Suloway, C., Pulokas, J., Fellmann, D., Cheng, A., Guerra, F., Quispe, J., Stagg, S., Potter, C.S., and
858 Carragher, B. (2005). Automated molecular microscopy: the new Leginon system. Journal of
859 structural biology *151*, 41-60.
860 Torrents de la Pena, A., Julien, J.P., de Taeye, S.W., Garces, F., Guttman, M., Ozorowski, G.,
861 Pritchard, L.K., Behrens, A.J., Go, E.P., Burger, J.A.*, et al.* (2017). Improving the Immunogenicity
862 of Native-like HIV-1 Envelope Trimers by Hyperstabilization. Cell Rep *20*, 1805-1817.
863 Turchaninova, M.A., Davydov, A., Britanova, O.V., Shugay, M., Bikos, V., Egorov, E.S., Kirgizova,
864 V.I., Merzlyak, E.M., Staroverov, D.B., Bolotin, D.A.*, et al.* (2016). High-quality full-length
865 immunoglobulin profiling with unique molecular barcoding. Nature protocols *11*, 1599-1616.
866 UNAIDS (2019). Global HIV & AIDS statistics — 2018 fact sheet.
867 van Beusekom, B., Wezel, N., Hekkelman, M.L., Perrakis, A., Emsley, P., and Joosten, R.P. (2019).
868 Building and rebuilding N-glycans in protein structure models. Acta Crystallogr D Struct Biol *75*,
869 416-425.
870 van Gils, M.J., van den Kerkhof, T.L., Ozorowski, G., Cottrell, C.A., Sok, D., Pauthner, M.,
871 Pallesen, J., de Val, N., Yasmeen, A., de Taeye, S.W.*, et al.* (2016). An HIV-1 antibody from an
872 elite neutralizer implicates the fusion peptide as a site of vulnerability. Nat Microbiol *2*, 16199.
873 Vigdorovich, V., Oliver, B.G., Carbonetti, S., Dambrauskas, N., Lange, M.D., Yacoob, C., Leahy,
874 W., Callahan, J., Stamatatos, L., and Sather, D.N. (2016). Repertoire comparison of the B-cell
875 receptor-encoding loci in humans and rhesus macaques by next-generation sequencing. Clin
876 Transl Immunology *5*, e93.

877 Wang, Y., O'Dell, S., Turner, H.L., Chiang, C.I., Lei, L., Guenaga, J., Wilson, R., Martinez-Murillo,
878 P., Doria-Rose, N., Ward, A.B.*, et al.* (2017). HIV-1 Cross-Reactive Primary Virus Neutralizing
879 Antibody Response Elicited by Immunization in Nonhuman Primates. J Virol *91*.
880 Williams, C.J., Headd, J.J., Moriarty, N.W., Prisant, M.G., Videau, L.L., Deis, L.N., Verma, V.,
881 Keedy, D.A., Hintze, B.J., Chen, V.B.*, et al.* (2018). MolProbity: More and better reference data
882 for improved all-atom structure validation. Protein science : a publication of the Protein Society
883 *27*, 293-315.
884 Wu, X. (2018). HIV Broadly Neutralizing Antibodies: VRC01 and Beyond. Adv Exp Med Biol *1075*,
885 53-72.
886 Xu, K., Acharya, P., Kong, R., Cheng, C., Chuang, G.Y., Liu, K., Louder, M.K., O'Dell, S., Rawi, R.,
887 Sastry, M.*, et al.* (2018). Epitope-based vaccine design yields fusion peptide-directed antibodies
888 that neutralize diverse strains of HIV-1. Nature medicine *24*, 857-867.
889 Yang, L., Sharma, S.K., Cottrell, C., Guenaga, J., Tran, K., Wilson, R., Behrens, A.J., Crispin, M., de
890 Val, N., and Wyatt, R.T. (2018). Structure-Guided Redesign Improves NFL HIV Env Trimer
891 Integrity and Identifies an Inter-Protomer Disulfide Permitting Post-Expression Cleavage.
892 Frontiers in immunology *9*, 1631.
893 Ye, J., Ma, N., Madden, T.L., and Ostell, J.M. (2013). IgBLAST: an immunoglobulin variable
894 domain sequence analysis tool. Nucleic Acids Res *41*, W34-40.
895 Yuan, M., Cottrell, C.A., Ozorowski, G., van Gils, M.J., Kumar, S., Wu, N.C., Sarkar, A., Torres, J.L.,
896 de Val, N., Copps, J.*, et al.* (2019). Conformational Plasticity in the HIV-1 Fusion Peptide
897 Facilitates Recognition by Broadly Neutralizing Antibodies. Cell Host Microbe *25*, 873-883 e875.
898 Zhang, K. (2016). Gctf: Real-time CTF determination and correction. Journal of structural biology
899 *193*, 1-12.
900 Zheng, S.Q., Palovcak, E., Armache, J.P., Verba, K.A., Cheng, Y., and Agard, D.A. (2017).
901 MotionCor2: anisotropic correction of beam-induced motion for improved cryo-electron
902 microscopy. Nature methods *14*, 331-332.
903 Zimin, A.V., Cornish, A.S., Maudhoo, M.D., Gibbs, R.M., Zhang, X., Pandey, S., Meehan, D.T.,
904 Wipfler, K., Bosinger, S.E., Johnson, Z.P.*, et al.* (2014). A new rhesus macaque assembly and
905 annotation for next-generation sequencing analyses. Biol Direct *9*, 20.
906 Zivanov, J., Nakane, T., Forsberg, B.O., Kimanius, D., Hagen, W.J., Lindahl, E., and Scheres, S.H.
907 (2018). New tools for automated high-resolution cryo-EM structure determination in RELION-3.
908 eLife *7*.
909

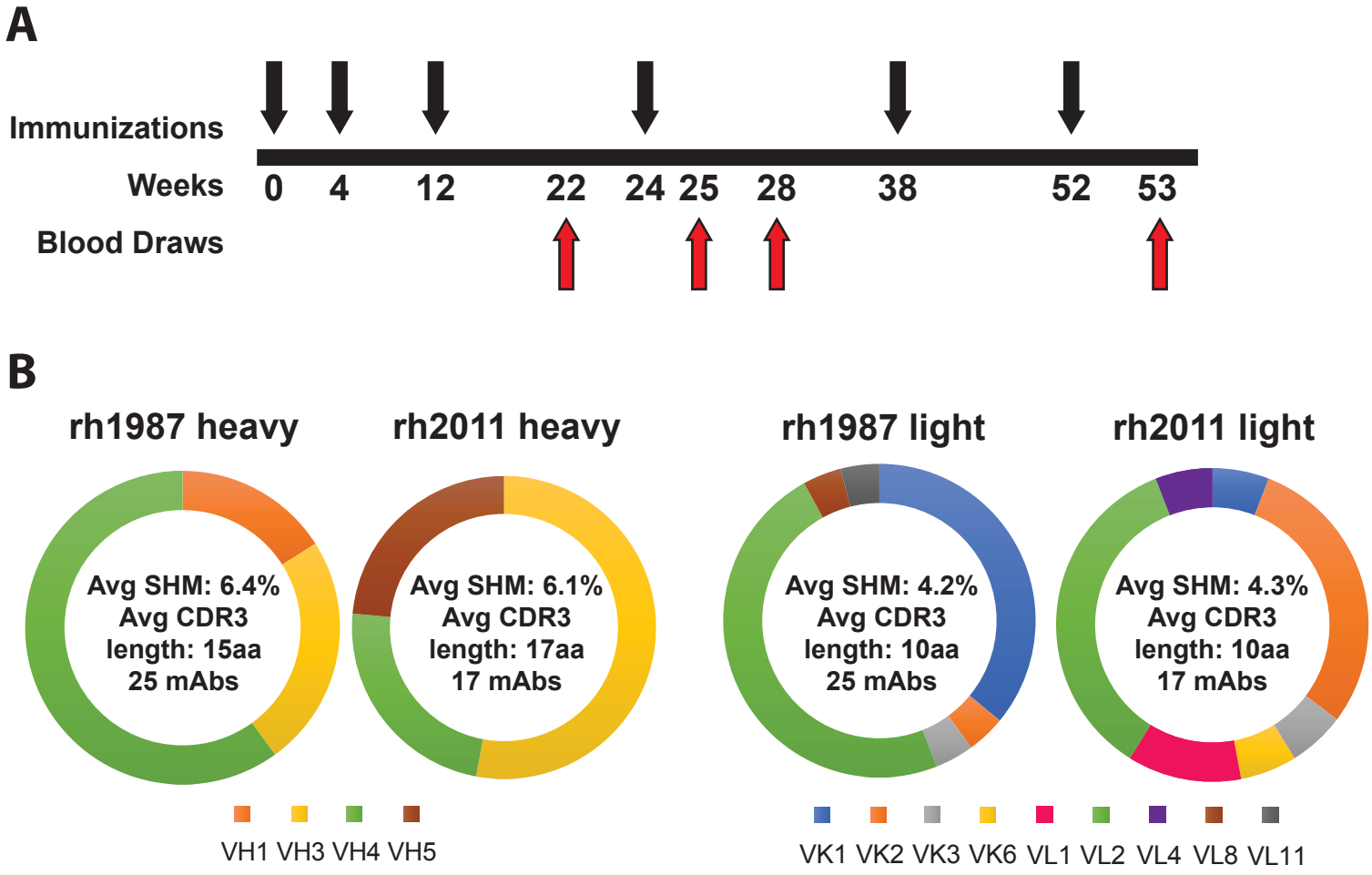

C

rh1987

mAb	BG505 T332N	BG505 T332N+N611A	SF162
RM19A	41.8	>50	>50
RM19A1	44.9	>50	>50
RM19A2	>50	>50	>50
RM19A3	>50	>50	>50
RM19B1	>50	>50	>50
RM19C3	>50	>50	>50
RM19C4	>50	>50	>50
RM19D	>50	>50	>50
RM19J	>50	>50	>50
RM19M	12.9	5.63	>50
RM19N	>50	>50	>50
RM19O	>50	25.5	>50
RM19P	23.5	>50	>50
RM19R	>50	>50	>50
RM19S	>50	3.51	>50
RM19T	>50	>50	>50

IC_{50} (µg/mL)

D

rh2011

mAb	BG505 T332N	BG505 T332N+N611A	SF162
RM20A3	>50	>50	>50
RM20B	>50	>50	>50
RM20C	>50	>50	>50
RM20D	>50	>50	>50
RM20E	>50	<0.41	>50
RM20E1	>50	<0.41	>50
RM20E2	>50	<0.41	>50
RM20E3	>50	<0.41	>50
RM20F	1.6	<0.41	>50
RM20H	42.9	<0.41	>50
RM20I	>50	>50	>50
RM20J	>50	>50	>50

IC_{50} (µg/mL)

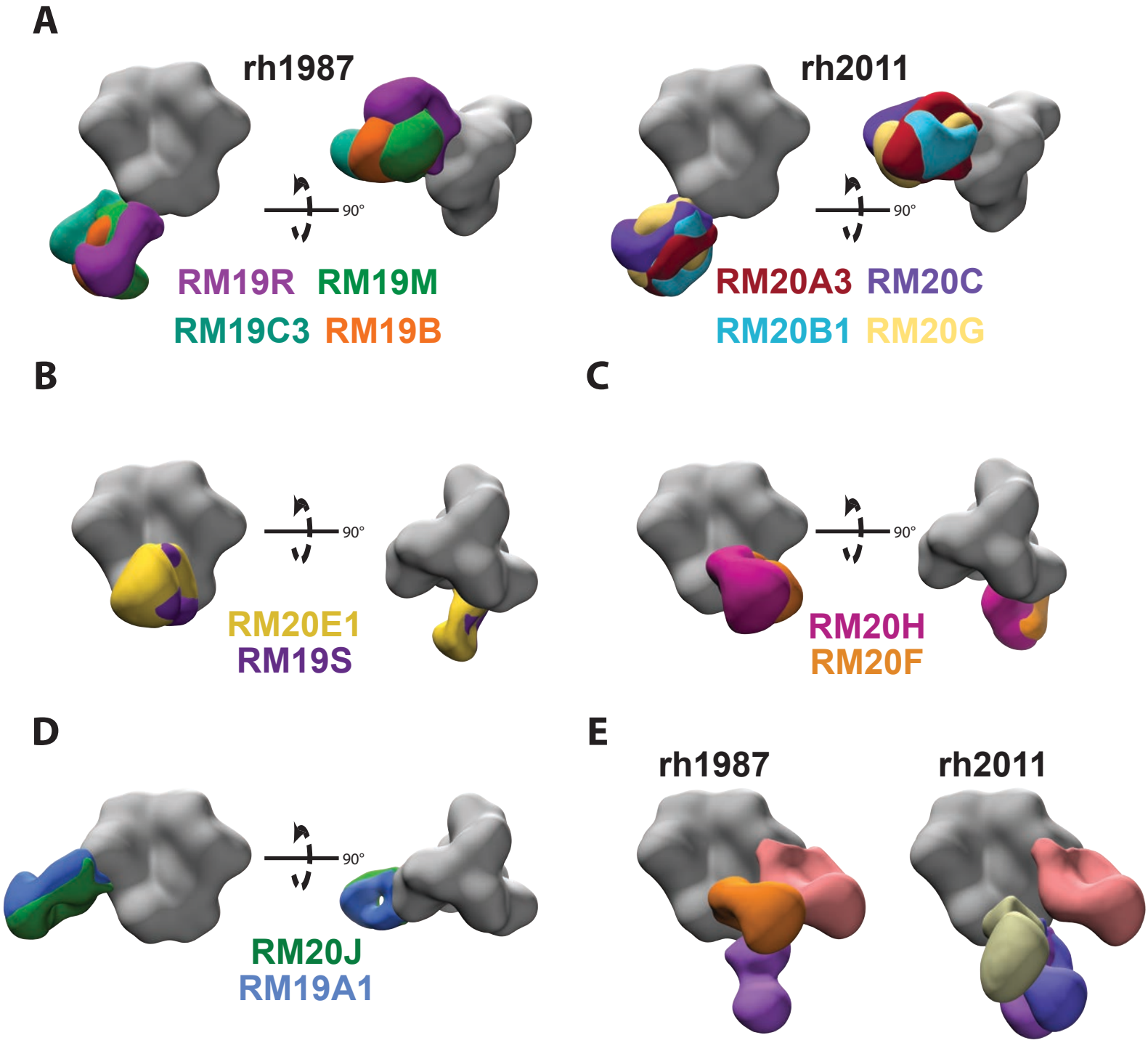
A
rh1987
90°
RM19R
RM19M
RM19C3
RM19B
rh2011
90°
RM20A3
RM20C
RM20B1
RM20G
B
90°
RM20E1
RM19S
C
90°
RM20H
RM20F
D
90°
RM20J
RM19A1
E
rh1987
rh2011

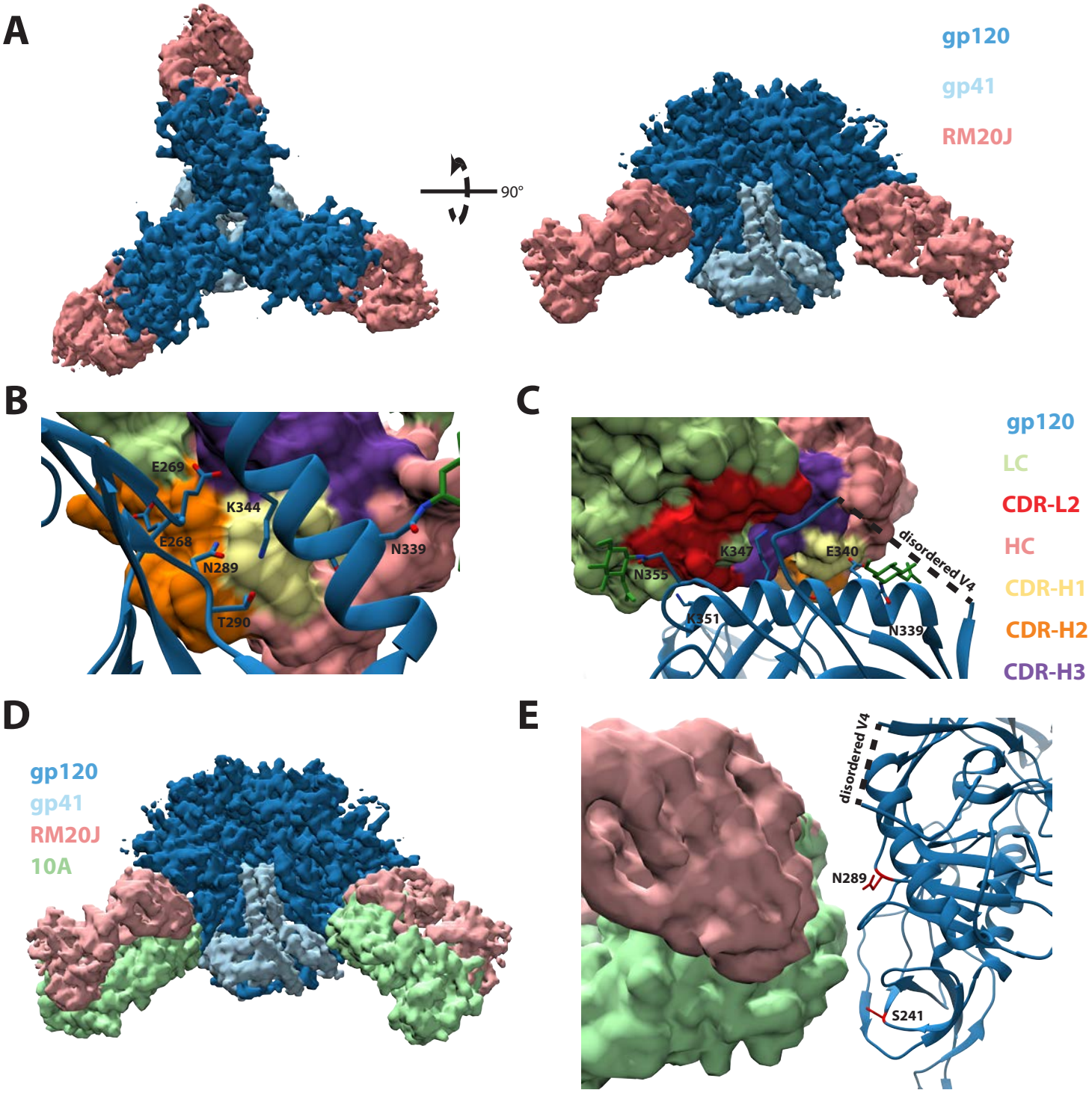
A
gp120
gp41
RM20J
90°
B
E269
K344
E268
N289
T290
N339
C
gp120
LC
CDR-L2
HC
CDR-H1
CDR-H2
CDR-H3
K347
E340
N355
K351
N339
disordered V4
D
gp120
gp41
RM20J
10A
E
disordered V4
N289
S241

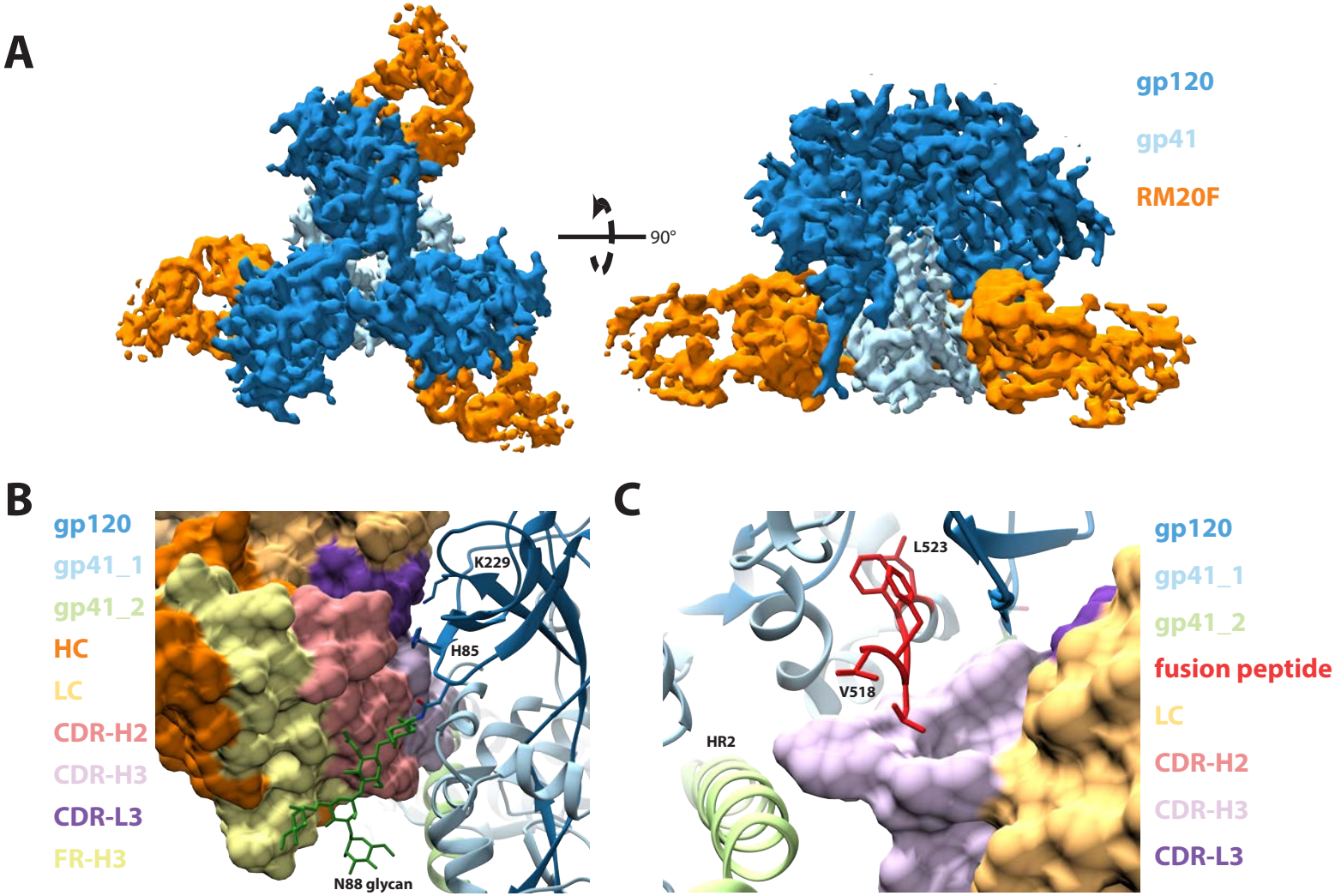

D

	VRC01	RM20F	VRC34
WT	1.0	1.0	1.0
H85A	1.2	11.9	4.7
E87A	1.2	4.3	0.8
N88A	1	>28	>24
K229A	0.6	3.1	1.2
S241N	1.1	6.6	n.d.
E267A	0.8	1.3	0.9
P291T	1.1	2.9	n.d.
N332T	0.9	0.5	n.d.
F522A	0.8	3.9	1.0
M535A	0.9	2.9	1.0
T536A	0.8	2.9	1.5
T538A	0.8	3.6	1.2
N611Q	1.5	<0.1	n.d.
N625Q	1.9	0.6	n.d.
N637Q	1.6	1.2	n.d.
G644A	1.0	4.2	1.8
E647A	1.7	13.5	0.6

fold reduction in neutralization

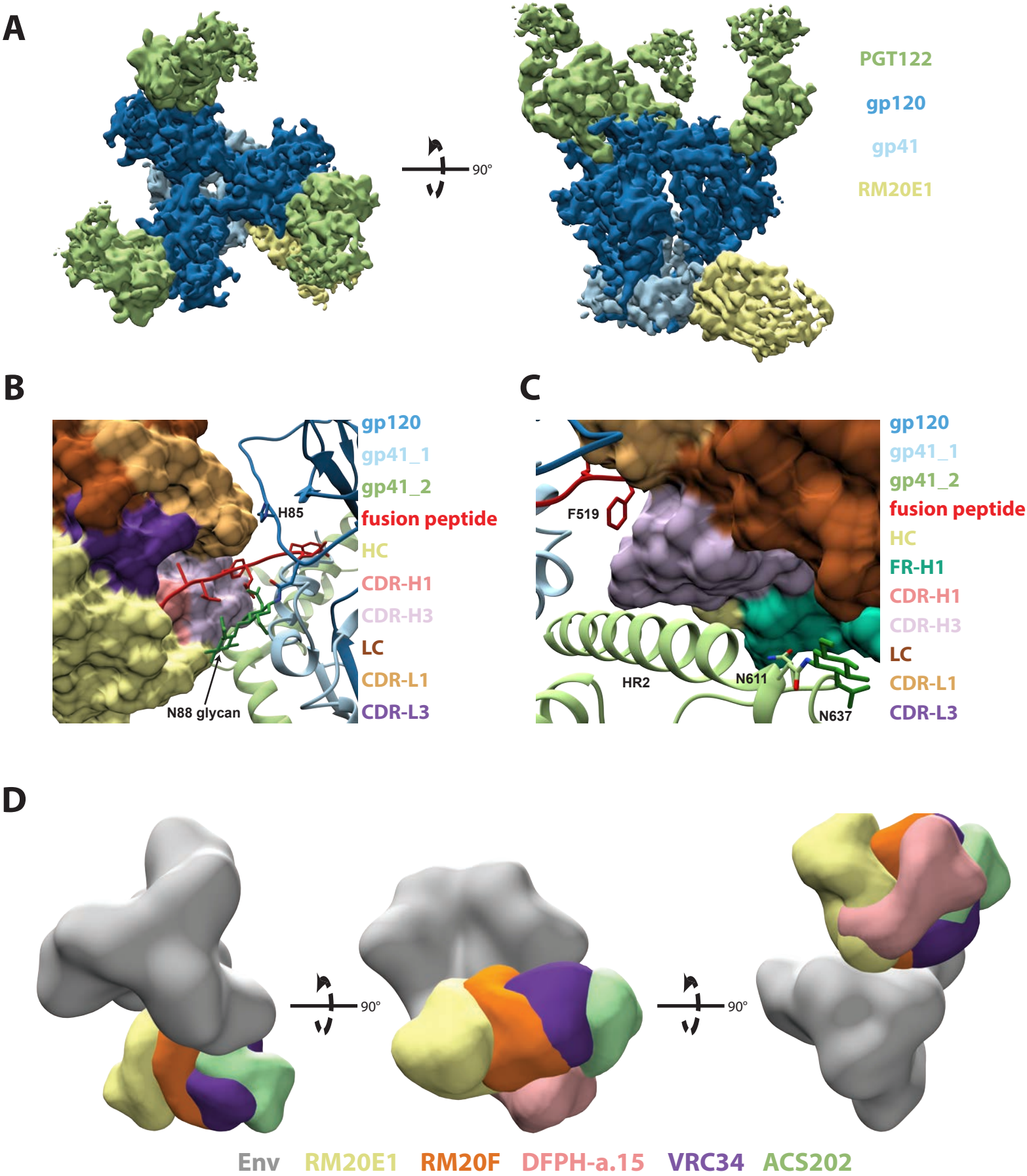
A
90°
PGT122
gp120
gp41
RM20E1
B
gp120
gp41_1
gp41_2
fusion peptide
HC
CDR-H1
CDR-H3
LC
CDR-L1
CDR-L3
H85
N88 glycan
C
gp120
gp41_1
gp41_2
fusion peptide
HC
FR-H1
CDR-H1
CDR-H3
LC
CDR-L1
CDR-L3
F519
HR2
N611
N637
D
90°
90°
Env
RM20E1
RM20F
DFPH-a.15
VRC34
ACS202